INVESTIGATING THE NOVEL ONCOGENIC FUNCTION OF SAPCD2 IN PEDIATRIC NEUROBLASTOMA

by

Amy Baker, B.S.

A thesis submitted to the Graduate Council of
Texas State University in partial fulfillment
of the requirements for the degree of
Master of Science
with a major in Biochemistry
August 2021

Committee Members:

Liqin Du, Chair

L. Kevin Lewis

Tania Betancourt

FAIR USE AND AUTHOR'S PERMISSION STATEMENT

Fair Use

Duplication Permission

DEDICATION

To my nieces, Adelyn and Elanor Fitzhenry, and my nephew Madden Zeal Ramos. May your curiosity about the world around you never be harnessed.

ACKNOWLEDGEMENTS

I would like to extend my sincerest gratitude to my PI, Dr. Liqin Du. She has provided me with unwavering support, patience, and encouragement since I first joined her lab as an undergraduate student in 2018. Throughout my time working with her, my confidence in myself and my ability to be successful beyond my time at Texas State has flourished as a result of her consistent warmth and empathy. Besides teaching me and helping me to refine nearly all of my hands-on laboratory skills, she also taught me the importance of rest, work-life balance, and growth mindset. She was able to recognize the times when I needed tough love and the times when I needed reassurance and has molded me into a better student and scientist. When speaking with my friends and classmates, I have often referred to her as my "science mom" due to her innate desire to support me in several different aspects of my life. I will forever carry with me the life lessons I have learned from her and will be forever grateful for the ways in which she has enriched my education.

I am grateful for my committee members, Dr. Lewis and Dr. Betancourt, for their guidance and feedback throughout the last two years. I would also like to thank my family for their support throughout my entire undergraduate and graduate education. I would especially like to thank my

parents for everything they have sacrificed to give me the opportunity to reach this point. They have helped me develop the skills I needed to be self-sufficient throughout graduate school and beyond and they are always willing to hear me talk about my research when I am excited about it, despite not having a background in biochemistry and probably finding a lot of my subject matter to be quite boring. My sisters Ashley Fitzhenry and Kelli Ramos, as well as my brothers-in-law Roby Fitzhenry and Micah Ramos, have consistently reminded me of the importance of knowing when to step away from my schoolwork and spend time with family.

I am very grateful for all of my close friends Samantha Chapman, Tori Cerar, Shea Toms, Casey Pruitt, and Xavier DeLaRosa for their humor, friendship, and company which has kept me sane throughout graduate school. I would like to thank Tori for all the movie nights and horseback riding that provided relief from the stress of academia. Samantha, Shea, Casey, and Xavier have made working in EMS alongside graduate school both fun and challenging, and all of them have consistently encouraged and promoted my decision to continue my education beyond my master's degree. I couldn't imagine having better people to run emergency calls with in the middle of the night and goof off with during the day when we get bored.

I would like to thank, recognize, and congratulate all of my classmates and friends through school for their support as peers who all understand the

unique stressors of graduate school in the STEM field. Not only have we conquered our master's program, we have all done it in the middle of a historical global pandemic. I am extremely impressed with everybody's tenacity and grit throughout the last two years as life threw us all every possible curveball. I have no doubt that each and every one of you will be highly successful in whatever direction you take after this year.

TABLE OF CONTENTS

Page

LIST OF TABLES

Table **Page**

LIST OF FIGURES

Figure **Page**

LIST OF ABBREVIATIONS

Abbreviation	Description
ALK	Anaplastic Lymphoma Kinase
APC/C	Anaphase-promoting complex/cyclosome
CDC	Cell division cycle
CDK	Cyclin-dependent kinase
Chk2	Checkpoint kinase 2
CNS	Central nervous system
CRC	Colorectal cancer
DCG	Dense core granule
DCLK1	Doublecortin-like kinase
DCX	Microtubule-associated doublecortin
dsRNA	Double-stranded RNA
EMT	Epithelial-Mesenchymal Transition
FWER	Family-wise error rate
GC	Gastric cancer
GI	Gastrointestinal
HCC	Hepatocellular Carcinoma
IRK	Insulin receptor kinase
LDL	Low-density lipoprotein
lncRNA	Long non-coding RNA
MAP	Microtubule associated protein
MCT	Multiple comparisons test

miRNA	MicroRNA
MRD	Minimal residual disease
NET	Neuroendocrine tumor
NPC	Nasopharyngeal carcinoma
NSCLC	Non-small cell lung cancer
ORF	Open reading frame
PKC	Protein kinase C
PP2A	Protein phosphatase 2
RAR	RA receptor
RBP	RNA-binding protein
RCC	Renal cell carcinoma
RISC	RNA-induced silencing complex
RNAi	RNA interference
RPC	Retinal progenitor cells
RTK	Receptor tyrosine kinase
RXR	Retinoid X receptor
SAC	Spindle assembly checkpoint
siRNA	Short interfering RNA
SNP	Single nucleotide polymorphism
UTR	Untranslated region

ABSTRACT

Pediatric neuroblastoma is the most common extra-cranial solid malignancy in infants and children. It is an aggressive neuroendocrine cancer that circumvents the normal differentiation process of sympathetic neuronal precursors into diverse cell types of the peripheral nervous system. SAPCD2 is a newly identified cell cycle-associated gene involved in mitotic progression and spindle assembly. Although the specific mechanism by which SAPCD2 modulates the cell cycle is poorly understood, its function appears to be most critical in early embryonic development where it regulates cell polarization, orientation, and fetal tissue segmentation. The expression of SAPCD2 is generally low or absent in healthy postnatal tissues, yet its abnormal restored expression in several adult cancers has been well documented and its oncogenic function has been supported by *in vitro* and *in vivo* investigations. Its relevance to neuroblastoma, however, has never been investigated. The objective of this thesis work is to determine whether high expression of SAPCD2 in neuroblastoma correlates with poor patient survival and, if so, to characterize its oncogenicity *in vitro* utilizing human neuroblastoma cell lines. Our results indicate that SAPCD2 functions as an oncogene in pediatric neuroblastoma that contributes to poor overall and recurrence-free survival. This effect likely results from the cellular effects that SAPCD2 possesses on neuronal precursors, including sustained proliferative signaling and evasion of growth suppressors.

However, SAPCD2 does not appear to play a significant role in inducing the differentiation of neuronal precursors. In the future, studies aimed at characterizing the effect of SAPCD2 on coordinating apoptotic pathways would complement the results of our current investigation and enrich the understanding of the role that SAPCD2 plays in tumorigenesis.

I. INTRODUCTION

Neuroendocrine tumors

Neuroendocrine tumors (NETs) arise in specialized tissues and organs known to possess functional characteristics of both nerve cells as well as hormone-producing cells. The presence of dense core granules (DCGs), which are involved in the transportation and secretion of neuropeptides in response to stimuli, is a defining feature of NETs and is responsible for the “neuro” designation of the name [1]. Although these DCGs are functionally important constituents of both neurons and neurosecretory cells, neuroendocrine cells do not contain axons or synapses and are incapable of establishing electrochemical signals between communicating cells [2, 3]. However, neuroendocrine tissues often possess the ability to produce and secrete peptide hormones in response to signals received from the nervous system, a trait that is usually imparted on neuroendocrine neoplasms [4]. Among some of the hormones commonly secreted by neuromodulating cells include neuron-specific enolase (NSE), 5-hydroxytryptamine (serotonin (5-HT)), and synaptophysin, which can cause severe side effects in patients with functional NETs that secrete an abnormally high amount of one or more hormones [5]. Due to the wide distribution of neuroendocrine tissues in the body, NETs are identified in a variety of primary sites such as within the central nervous system (CNS), gastrointestinal (GI) tract, thyroid, and pulmonary system. The most frequently identified primary site of NETs are the GI tract (62%-67%), and the lung (22-27%) [6]. Clinical detection is

more common at advanced disease stages due to the tendency of NETs to be asymptomatic in early stages, and metastatic tumors exist in 12%-22% of patients at the time of diagnosis [6].

NETs are generally classified as well differentiated (tumors which are identified by the presence of abundant neuroendocrine markers such as synaptophysin and chromogranin A) or poorly differentiated (tumors in which the levels of synaptophysin and chromogranin A are diffuse or absent), designations that reflect the extent to which particular tumors have retained stem cell characteristics [2]. The ability of NETs to retain such characteristics enables them to achieve a highly aggressive phenotype and intensifies genomic instability, which enable the cells to evade growth suppressors and sustain proliferative signaling. While most NETs have been shown to be modestly chemosensitive, the dynamic nature of poorly differentiated tumors presents a clinical challenge in developing effective treatments. Currently, poorly differentiated NETs have a median 2-year survival rate less than 20% [7].

Neuroblastoma

Pediatric neuroblastoma is an aggressive neuroendocrine cancer of the adrenal glands that is most commonly diagnosed in infants and children less than nineteen months of age. It is an embryonic malignancy that arises from the failure of sympathetic neuronal precursors to fully differentiate into normal diverse cell types such as peripheral neurons, enteric neurons and glia, and melanocytes [8-10]. The adrenal glands are triangular-shaped retroperitoneal structures located on top of each kidney and are composed of an outer cortex,

which functions to secrete glucocorticoids, aldosterone, and androgens, and an inner medulla which functions to secrete catecholamines [11]. The outer cortex of the adrenal glands originates from the mesoderm during embryonic development and is an extension of the autonomous nervous system [11]. It plays an important role in the renin-angiotensin-aldosterone system to maintain cardiovascular homeostasis and utilizes cholesterol through low-density lipoprotein (LDL) receptors on the surface of the adrenal tissue to synthesize steroid hormones [12]. The secretion of glucocorticoids from the cortex functions to modulate glycogen, protein, and lipid metabolism [12]. Past studies have indicated that cells migrate from the outermost region of the cortex towards the inner region during differentiation, before senescing near the cortex-medulla border [13-15]. The secretion of catecholamines from the inner medulla occurs in response to signals received from the hypothalamus, stimulating the sympathetic nervous system to react to an external stimulus. This phenomenon is often referred to as the “fight or flight” response and controls heart rate and respiratory rate during acute stress events.

Neuroblastoma disrupts adrenal function by creating pathophysiological variations in primordial hormone-producing cells. The development of neuroblastoma is thought to be prenatal in origin, arising from the deregulated construction of the embryonic neural crest **(Figure 1)** [8, 9]. This important multipotent structure, which arises from the convergence of the epidermal ectoderm and the neuroectoderm, forms the central nervous system (CNS) and predates many diverse cell types of the sympathetic and peripheral nervous

systems [9, 16]. Neural crest development begins during gastrulation and is coupled with development of the neural tube, which gives rise to the brain and spinal cord [9, 16]. The migration of neural crest cells into diverse locations in the body initiates differentiation into specialized cells and tissues such as

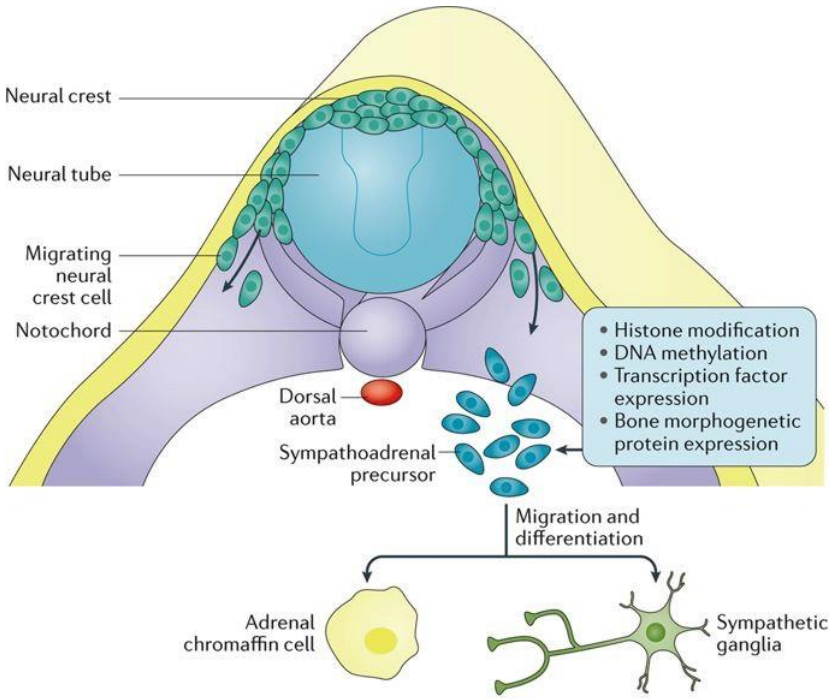

Figure 1. Early Formation of the Neural Crest. During gastrulation in vertebrate embryos, the neural tube develops from invagination of the neural plate and will give rise to the CNS: the cortex, brainstem, and spinal cord. The dorsal neural crest cells will migrate throughout the entire body and differentiate into a wide variety of cells. The notochord is a midline structure that secretes sonic hedgehog patterning signals to surrounding tissues, and the dorsal aorta will develop vessels along the longitudinal axis to perfuse the embryo [8].

mesenchymal, neuronal, secretory, and pigmented cells [10]. Components of the neural crest also give rise to craniofacial skeletal structures, adrenal chromaffin cells, and sensory neurons [17]. Due to their multipotent nature, the cells of the

neural crest possess enhanced migratory and replicative capabilities [18]. The initiation and progression of neural crest development is a tightly controlled, complex process involving a diverse orchestration of gene regulatory networks and transcription factors [19]. Dysregulation of this process can have serious implications for developing embryos and can give rise to pathogenic neuroblasts [9]. Approximately 60% of primary neuroblastoma tumors are identified in paravertebral ganglia, while 30% of primary tumors originate in the adrenal medulla, and the remaining cases are identified in other various sympathetic ganglia originating from the neural crest **(Figure 2)** [20]. Neuroblastoma occurs

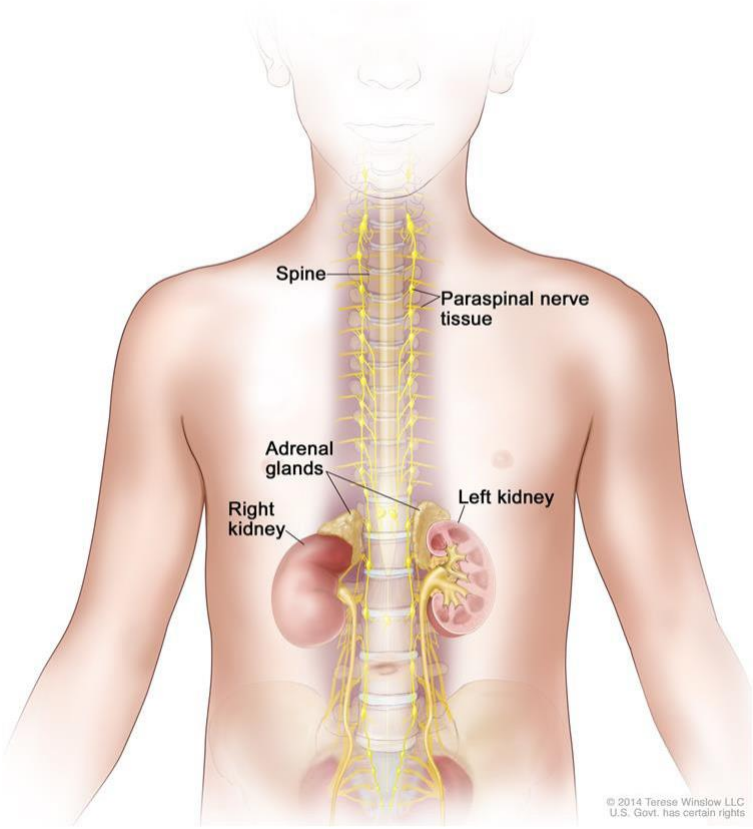

Figure 2. Common Neuroblastoma Primary Tumor Sites. Approximately 60% of primary tumors arise within the paravertebral ganglia, 30% within the adrenal glands, and 10% in various other sympathetic ganglia originating from the neural crest [20].

almost exclusively in infants and young children, an observation that corroborates the proposal of its prenatal origins [8]. Neuroblastoma is a heterogenous disease that exhibits a wide range of clinical presentations upon diagnosis. The tendency for primary tumors to arise in several different areas with highly variable genetic profiles presents a clinical challenge in developing therapies that are effective for a large number of patients. There exists great diversity in the outcomes of neuroblastoma patients, ranging from spontaneous regression without clinical intervention to highly aggressive phenotypes resistant to chemotherapy and radiation [21]. Tumor aggressiveness depends largely upon differentiation status at the time of diagnosis. Patients with tumors exhibiting poor differentiation typically have poorer outcomes than those with better-differentiated tumors [20, 22]. Additionally, amplification of the proto-oncogene MYCN at the chromosomal level is famously correlated with markedly reduced overall and event-free survival of neuroblastoma patients [22]. MYCN amplification in neuroblastoma is among the most consistent indicators of treatment failure and MYCN status is a major factor in risk group stratification of neuroblastoma patients [22]. The N-myc translation product of MYCN is a transcription factor that promotes cell proliferation and metabolism and is vitally important to developing embryos. Its amplification is associated with various additional developmental malignancies of childhood onset including medulloblastoma, rhabdomyosarcoma, and Wilms' tumor [23].

In addition to MYCN amplification, gain-of-function missense mutations in ALK, encoding Anaplastic Lymphoma Kinase (ALK) receptor, are associated with

poor outcomes in approximately 14% of high-risk neuroblastoma patients [24]. ALK is a receptor tyrosine kinase (RTK) in the insulin receptor kinase (IRK) superfamily thought to possess important functions throughout embryonic development by regulating neuronal proliferation [24]. Cluster missense mutations within important regulatory regions of ALK lead to autophosphorylation and ligand-independent signal transduction [24, 25]. A small-molecule inhibitor of ALK, patented under the name *crizotinib*, was approved in 2011 for use in non-small cell lung cancer (NSCLC) and showed promising results in some neuroblastoma patients [24, 26, 27]. Downregulation of ALK expression via RNA interference (RNAi) has likewise led to a reduction in neuroblastoma cell proliferation *in vitro* [28]. Current therapeutic interventions for neuroblastoma include the use of vitamin A derivative 13-cis-retinoic acid, a synthetic differentiation-inducing retinoid compound that has demonstrated great success in stalling tumor enlargement in some patients with poorly differentiated tumors **(Figure 3)** [29]. The retinoic acid receptor families RA receptor (RAR) and retinoid X receptor (RXR) are thought to be expressed on the surfaces of most neuroblastoma cells and mediate the differentiation function stimulated by retinoids [30]. Both RAR and RXR belong to the thyroid hormone family of receptors and host the interaction between retinoid compounds and specific DNA sequences known as retinoic acid response elements through conformational changes [29]. RAR and RXR mutational changes to not appear to be major mechanisms through which neuroblastoma cells acquire resistance against retinoids, although the probed overexpression of these receptors may increase tumor sensitivity to

retinoid compounds [29]. Combination therapy including retinoids has been shown to be more effective in treating neuroblastoma than the use of retinoids alone [30]. Administration of 13-cis-retinoid acid in conjunction with aggressive chemoradiation therapy and bone marrow transplant has improved survival for

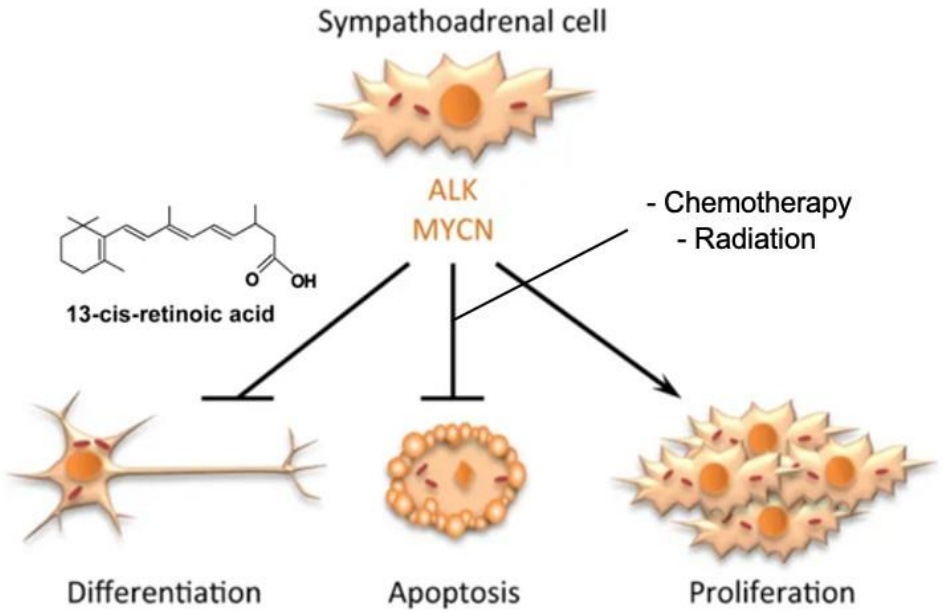

Figure 3. Possible Outcomes of Malignant ALK/MYCN Transformed Cells. Current differentiation therapy utilizing 13-cis-retinoic acid induces the formation of terminal neurons ***(left)***, while traditional anti-cancer therapies target proliferation pathways and induce cell cycle arrest and apoptosis ***(center)***. In the absence or failure of clinical intervention, malignant transformed cells enhance proliferative signaling ***(right)*** [23, 28].

35% of high-risk patients, yet only half of these patients remain recurrence-free for five years [31-33]. The use of traditional anti-cancer strategies such as chemotherapy, radiation, and surgical resection without additional differentiation therapy are largely unsuccessful due to persistent minimal residual disease (MRD) [31]. Overall, the modest success rates of aggressive treatment regimens are a direct result of the heterogeneity of neuroblastoma and the diverse genetic

profiles of each individual case. Rigorous investigation into the mechanism driving the onset and progression of neuroblastoma as well as the identification of novel neuroblastoma-associated oncogenes are therefore important to the development of improved drug targets.

The Cell Cycle and Cancer Development

Aberrant regulation of the cell cycle has long been associated with tumorigenicity [34]. Studies investigating the complexity of this pathway and its many constituents have focused on describing the mechanisms of cell cycle control through cofactors, allosteric regulation, and feedback inhibition. Several important checkpoints within the cell cycle have been well characterized, including the spindle assembly checkpoint (SAC), which controls mitotic progression [35, 36]. The SAC is of particular interest due to its involvement in regulating the formation of cellular scaffolds such as microtubules, spindle proteins, and centromeric proteins. When pathophysiological variants within these important cellular scaffolds are detected, the SAC blocks cell division by inhibiting CDC20, the cofactor of the E3 ubiquitin-ligase anaphase-promoting complex/cyclosome (APC/C). Down-regulation of this large protein complex prevents the destruction of two important substrates required for the progression to anaphase, cyclin B and securin [37]. The active cyclin B/CDK-1 complex, also called the mitotic promoting factor, advances mitotic progression and is detected in very high amounts during late G_2 phase and early M phase before abruptly falling upon initiation of G_1. Securin is a key APC/C substrate that binds to and blocks the action of separase, preventing the premature separation of sister

chromatids and stalling the transition to anaphase [38].

Cell Cycle Regulators in NETs and Neuroblastoma

The role of cell cycle-regulating proteins in the development and progression of NETs is poorly understood. Yet, a few cell cycle-modulating proteins have been implicated in various malignant neuroendocrine neoplasms, including the cyclin-dependent kinase inhibitor CDKN1B [39]. Somatic mutations occurring in CDKN1B have been documented in several cases of NETs of the small intestine, and loss of CDKN1B function is known to contribute to poor prognosis in several NETs involving the GI tract [39-44]. Loss of function mutations occurring in CDKN1B causes a corresponding reduction in cyclin dependent kinase inhibitor 1B (p27), releases inhibition on the cyclin B-Cdk complex, and enhances G_2-M phase progression.

The role of cell cycle-promoting genes in the progression of neuroblastoma has also been investigated. Mitotic spindle assembly and chromosomal segregation are tightly controlled processes that are required for the maintenance of normal cell cycle progression, and the dysregulation of these processes during mitosis appear to play a particularly large role in the onset and progression of neuroblastoma and gliomas [45]. Specifically, microtubule-associated proteins (MAPs), especially those encoded by alternative splice variants of the doublecortin-like kinase gene (DCLK1), are upregulated in neuroblastoma and glioma and contribute to neuroblast proliferation [46]. The NUSAP1 gene is another MAP that is essential for neural crest migration in

zebrafish [45]. DCLK1 is one of the many proposed gene targets in the treatment of neuroblastoma, recognized for its effects in regulating neuronal proliferation, migration, and neurogenesis [46]. DCLK1-derived MAPs are involved in cell cycle regulation, cell fate determination, and neuronal migration and are especially important in neurogenesis, where they are heavily involved in mitotic spindle formation [47-50].

The function of microtubule stabilization by DCLK1-associated MAPs is comparable to that of the microtubule-associated doublecortin (DCX) gene involved in neuronal migration [47]. DCX is expressed in neuroblastoma as a biomarker for persistent MRD [51]. Furthermore, many studies have indicated that expression changes (depletion or overexpression) in DCX family MAPs can decelerate cellular proliferation by disruption of the mitotic spindle [47, 48, 52, 53]. In addition to MAPs, several other protein-coding genes involved in cell cycle regulation have been associated with neuroblastoma. For example, cyclin-dependent kinases (CDKs) 4 and 6 form a complex with cyclin D and promote G_1/S cell cycle progression and inhibition of CDK4/6 has been demonstrated to be a promising therapeutic option for the treatment of neuroblastoma [54]. The role of cell cycle regulating genes in neuroblastoma differentiation has recently been summarized [55].

The SAPCD2 Gene and its Protein Product

SAPCD2 (NCBI Gene ID 89958) is a cell cycle-dependent gene that is highly expressed in embryonic tissues. It is located on the long arm of

chromosome 9 at position 34.3 in *Homo sapiens* and its full-length cDNA is approximately 4.0 kb [56]. It encodes a 389 amino acid protein product estimated to be 42.3 kDa, inspiring its common alias p42.3 [57]. An additional alias, c9orf140, has also been established. Although the complete protein structure of SAPCD2 has yet to be illustrated, some significant features have been identified. The upstream region of the SAPCD2 open reading frame (ORF) contains a Kozak consensus sequence and its coding region consists of seven exons [57]. The translation product of SAPCD2 mRNA contains numerous potential phosphorylation sites for checkpoint kinase 2 (Chk2) and protein kinase C (PKC), as well as some important second messengers such as cAMP and cGMP [57]. The N-terminus contains an EF-hand motif and the C-terminus is characterized by a coiled-coil (CC) domain which may interact with other proteins [57]. The EF-hand domain is a helix-loop-helix motif characterized by a calcium-binding chelate ring flanked by two alpha helices [58]. EF-hand domains are commonly found within the S100 oncoprotein family, which contain several low molecular weight calcium-binding proteins [59]. The primary sequence encoding these calcium-binding proteins is highly conserved in vertebrates and may provide hints about the function of SAPCD2 [59]. In 2015, Liu et al. created a 3D ligand binding model of the EF-hand motif within SAPCD2 and predicted metal ion binding sites at Ala78, Ser79, Tyr81, and Arg86. The EF-hand structural motif existing at the N-terminus of SAPCD2 suggests the possible involvement of SAPCD2 with the tumor-related calcium binding S100 family, many of which exist as homodimeric proteins intricately involved in the calcium-dependent modulation of proliferation

and differentiation [60]. The SAPCD2 protein also includes multiple proline-rich regions, which may mediate protein-protein interactions [57].

The presence of potential phosphorylation sites for Chk2 and PKC within SAPCD2 strongly suggests that it may play a key role in regulating cell proliferation throughout fetal development by modulating the signal transduction pathways for a variety of processes including cell cycle progression. The serine/threonine protein kinase Chk2 is a tumor suppressor that regulates cell cycle checkpoint arrest through phosphorylation of several mitotic phase-inducing cell division cycle (CDC) phosphatases. When DNA damage or mutations are detected, the phosphorylation of CDC phosphatases by Chk2 inhibits their mitotic-promoting activity and stalls cell cycle progression. PKC is a family of 15 isozymes composing three subfamilies (classical, novel, and atypical) that are defined by the second messengers required for activation. The classical PKCs, which are the most divergent from the original PKC in *Saccharomyces cerivisiae*, contain the α, β_{I}, β_{II}, and γ isoforms and require Ca^{2+}, diacylglycerol (DAG), and a phospholipid for activation [61]. PKCs play critical roles in cellular regulation and signal transduction. Although the direct role of PKCs in oncogenesis is poorly defined, the oncogenic potential of some PKC-mediated processes have been described [62]. For example, the expression level of the PKC isozyme PKCα is associated with the transformation of stem cells from the epithelial phase to the mesenchymal phase with a corresponding detachment from the basal membrane and acquired migration capacity [63]. This phenomenon is characteristic of oncogenic stem cell behavior and imparts a

major influence on tumor aggressiveness.

Current Understanding of SAPCD2 Function

Since the initial discovery of this gene in a gastric cancer cell line in 2007, increasing evidence has suggested that its functions extend beyond that of regulating cell cycle progression to include modulation of cell fate throughout fetal development. The expression level of SACPD2 is high throughout embryogenesis but is generally absent in healthy postnatal tissues, while its restored expression in adult tissues has been associated with various disease states. Additionally, the recently identified SAPCD2 protein interplay network suggests that the cellular functions of SAPCD2 are likely more diverse than currently recognized [64]. The pathological consequences of its aberrant expression have also been investigated, most notably in the initiation of several cancers. A role for SAPCD2 in tumorigenesis has been supported by *in vitro*, *in vivo*, and clinical retrospective investigations, and the underlying mechanisms driving this function have been partially elucidated. However, many questions pertaining to its detailed mechanism of oncogenic action as well as its potential as a diagnostic factor and therapeutic target remain to be investigated in future studies. In addition to its apparent function as an oncogene, previous investigations have suggested the involvement of SAPCD2 in other pathological processes such as inflammation, pointing out additional directions that warrant future investigation.

The Role of SAPCD2 in Tumorigenesis

The expression of SAPCD2 is high throughout embryonic development but is generally diffuse or absent in healthy postnatal tissues. However, its higher expression level is restored in several adult malignancies, suggesting that it plays an oncogenic role when expressed beyond early development. Indeed, several studies have indicated that SAPCD2 overexpression promotes the oncogenic transformation of several different types of cancers **(Table 1)**.

Table 1. Summary of SAPCD2 studies in cancers

Cancer Type	Specific Findings	Reference
Gastric cancer (GC)	Silencing of SAPCD2 reduces GC cell survival and proliferation	[57, 64-66]
Colorectal Carcinoma (CRC)	Contributes to CRC cell migration and invasion	[67, 68]
Nasopharyngeal Carcinoma (NPC)	Contributes to NPC cell migration and invasion	[69]
Melanoma	Contributes to melanoma proliferation, migration, and invasion	[70]
Renal Cell Carcinoma (RCC)	Contributes to RCC proliferation and invasion	[71]
Hepatocellular Carcinoma (HCC)	Overexpression upregulates PCNA, cyclin B1, and MAD2; advances tumorigenicity *in vitro* and *in vivo*	[72]

SAPCD2 in Gastric Cancer

SAPCD2 was first identified in 2007 by Xu et al. as a novel oncogene contributing to the progression of gastric cancer. The group originally reported changes to the expression levels of important cell cycle modulators Chk2 and

cyclin B1 following knockdown of SAPCD2 *in vitro*, which suggests the involvement of SAPCD2 in mitotic progression potentially by promotion of cyclin B/CDK-1 complex formation [57]. Since the original report, several other groups have further characterized its various roles in contributing to gastric cancer tumor aggressiveness [59, 66, 73, 74]. Liu et al. reported an upregulation of tumor suppressor Chk2 and downregulation of mitotic promoting factor cyclin B1 following SAPCD2 knockdown *in vitro*. The group deduced the highest probable regulatory pathway of SAPCD2 through Bayesian inference in the pathogenesis of gastric cancer to be S100A11 – RAGE – p38 – MAPK – microtubule associated protein – spindle protein – centromere protein – cell proliferation [59, 74]. Additionally, Hao et al. demonstrated that the levels of p42.3 and S100A11 are positively correlated in gastric cancer cells, further supporting early predictions that the protein product of SAPCD2 may interact with the S100 oncoprotein family based on a structural correlation [74]. Cao et al. further contributed to the previous findings by demonstrating that SAPCD2 overexpression is also correlated with cell proliferation, migration, and invasion in gastric cancer [66].

SAPCD2 in Colorectal Cancer, Hepatocellular Carcinoma, and Gliomas

SAPCD2 has been further identified as a possible biomarker for colorectal cancer (CRC) [75]. The expression level of SAPCD2 was reported to be significantly elevated in CRC tissues compared to health epithelial tissues and promotes cell proliferation, migration, and invasion *in vitro* [67]. Furthermore,

immunohistochemical staining of CRC cells expressing SAPCD2 revealed that SAPCD2 expression is related to unique clinicopathological characteristics and SAPCD2 knockdown suppressed CRC tumor growth *in vitro* [67]. Other studies have also reported a negative correlation between SAPCD2 expression and tumor differentiation in CRC [76]. The same group further reported that SAPCD2 expression is associated with poor prognosis in CRC patients, although this finding was not reproducible in later studies [67, 76]. Further elucidation of the genomic relationship between SAPCD2 expression level and prognosis of CRC patients is warranted. Hao et al. suggested in 2017 that the SAPCD2 protein product likely regulates apoptotic pathways in CRC cell lines through the FKBP – Bcl-2 – BAX – caspase-9 – caspase-3 pathway [68]. Bcl-2 is an anti-apoptotic protein that is upregulated in response to SAPCD2 depletion, while BAX is a pro-apoptotic protein that is downregulated in response to SAPCD2 depletion [68].

In addition to its contribution to the oncogenic transformation and progression of gastric cancer and CRC, SAPCD2 has also been identified as a driving factor in the tumorigenicity of hepatocellular carcinoma (HCC) [72]. HCC is the 5th most common cancer worldwide and is the third leading cause of cancer-related deaths [77]. Sun et al. reported that SAPCD2 is differentially expressed in primary hepatocellular carcinoma tumors and cell lines. Interestingly, just under 70% of screened HCC cells were positive for SAPCD2 expression, while 30% of healthy tumor-adjacent tissues were positive for SAPCD2 expression [72]. Similar to findings in other cancers, a significant correlation exists between SAPCD2 expression level and tumor differentiation in

HCC. Furthermore, expression level is positively associated with enhanced HCC cell growth and colony formation *in vitro*, a finding that was further reinforced by a measurable increase in tumorigenicity in nude mice [72]. No significant relationship was established between SAPCD2 expression level and other factors contributing to HCC, such as viral Hepatitis B status [72]. The effects of SAPCD2 expression on tumorigenicity in HCC can therefore be predicted to be independent of other common driving factors of HCC development.

In addition to its relevance in gastric cancer, CRC, and HCC, an additional study has reported that SAPCD2 is also overexpressed in glioma tumor tissues, in which is it positively associated with the degree of malignancy in gliomas [78]. The authors further suggested that the relationship between SAPCD2 expression level and malignancy of gliomas is compelling enough to suggest that SAPCD2 expression level may be a useful biomarker to grade glioma tumors [78].

SAPCD2 and Tumor Metastasis

SAPCD2 may also play an important role in tumor metastasis. Recent studies have demonstrated that knockdown of SACPD2 expression induces a decrease in neuronal (N)-cadherin and increase in calcium-dependent epithelial (E)-cadherin expression levels, which are involved in the regulation of cell adhesion and mobility [79]. Additional studies have corroborated these findings, showing that expression of SAPCD2 is positively correlated with β-catenin and p-ERK and negatively correlated with E-cadherin in gastric cancer [66]. Liu et al. demonstrated that SAPCD2 knockdown inhibits proliferation, migration, and

invasion in melanoma cells with an influence on the P13K/Akt pathway, MAPK pathway, and β-catenin [70]. Furthermore, SAPCD2 knockdown decelerates epithelial-mesenchymal transition (EMT) progression and decreases β-catenin activation in human renal cell carcinoma (RCC) [71]. SAPCD2 knockdown in RCC significantly stimulates the expression of E-cadherin and represses the expression of N-cadherin *in vitro* [71]. The transition from high expression levels of E-cadherin to high expression levels of N-cadherin are trademarks of aggressive tumor growth and stimulates initiation of the EMT. Although this process is essential during embryonic development and tissue regeneration, the selective stimulation in malignant transformed cells allows the ability for these cells to migrate unpredictably from their primary tumor site to distant locations in the body. Metastasis is famously associated with poor prognosis and is strongly associated with treatment failure as malignant cells become anatomically diffuse and challenging to target [80]. This important finding illustrates the ability of SAPCD2 to influence the metastatic cascade that often promotes tumors from early to advanced stages.

Cellular Function of SAPCD2

While the molecular functions of SAPCD2 within fetal development are poorly understood, some progress has been made in partially elucidating some of the various functions is appears to have within both normal and pathological processes **(Table 2)**. In an investigation aimed at elucidating the mechanisms controlling spindle orientation in retinal progenitor cells (RPCs), a key event

during the development of vertebrate regina, Chiu et al. revealed that SAPCD2 functions as a negative regulator of the Gαi-LGN-NuMA complex by interacting with several tight junction and polarity proteins including the LGN protein (also named G Protein Signaling Modulator 2, GPSM2) that are differentially regulated throughout development [81]. The Gαi-LGN-NuMA complex is an important regulator of spatiotemporal localization of cellular scaffolds throughout embryonic development, yet the mechanism through which it achieves this function remains to be fully elucidated [81, 82]. Co-immunoprecipitation experiments have revealed that SAPCD2 interacts with the tetratricopeptide repeat (TPR) within the N-terminal region of LGN, which is a region known to bind NuMA. Indeed, NuMA inhibits SAPCD2 binding to LGN in a dose-dependent manner, yet the inverse interactions has not been investigated [81]. Loss of SAPCD2 function randomized spindle orientation, and SAPCD2$^{-/-}$ clones promotes asymmetric terminal divisions in retinal progenitor cells (RPCs), producing bipolar neurons, amacrine neurons, or Müeller glial cells [81]. Additionally, the Gαi-LGN complex appears to be especially important for controlling progenitor orientation in neuroepithelial cells, which are responsible for the early formation of neurons [83, 84]. The interaction of SAPCD2 with these proteins plays an important role in balancing the proportion of horizontal and vertical divisions, and, consequently, symmetric and asymmetric cell divisions.

Table 2. Summary of the cellular functions of SAPCD2

Function	Targeting Molecules	Mechanism(s)	Reference
G_2/M Progression	Cyclin B1 Cdc2	↑ Cyclin B1 expression ↓ Cdc2 phosphorylation at Tyr15	[64]
Apoptosis	FKBP Bcl-2	↑ FKBP expression, stalls apoptosis ↓ Bcl-2 expression, stalls apoptosis	[68]
Wnt/β-catenin Signaling	Axin-1	Outcompetes PP2A for binding to Axin-1 ↓ Wnt/β-catenin Signaling	[85]
Mitotic Spindle Orientation	LGN	Negatively regulates LGN localization at cell cortex	[81]
Epithelial-Mesenchymal Transition (EMT)	E-cadherin N-cadherin β-catenin	↓ E-cadherin expression ↑ N-cadherin expression ↑ β-catenin expression	[71]
Cell Migration	?	↑ Cell Migration	[67]
Cell Invasion	?	↑ Cell Invasion	[67]

Despite its involvement in normal developmental processes, SAPCD2 likely possesses an oncogenic function when overexpressed beyond the early embryonic development of the neuroepithelium [64]. The high expression level of this gene in undifferentiated or poorly differentiated tissues corroborates its importance in cell cycle progression due to the high proportion of rapidly dividing cells throughout stem cell progression. These results suggests that SAPCD2 is a critical regulator of microtubule and mitotic spindle assembly.

A different group uniquely suggested in 2018 that SAPCD2 actually performs a different cellular function. Jiang et al. identified the SAPCD2 translation product as an Axin1-interacting protein, mediating the negative feedback loop of the proliferative Wnt/β-catenin signaling pathway through

association with the cytoplasmic destruction complex comprised of Axin1, APC, casein kinase 1 (CK1), and glycogen synthase kinase 1 (GSK1) [85]. This pathway modulates pluripotency and cell fate decisions throughout development and is functionally important during embryogenesis. Dysregulation of this pathway is implicated in some birth defects and developmental abnormalities in humans [86]. GST pulldown and co-immunoprecipitation experiments have suggested that the SAPCD2 protein outcompetes protein phosphatase 2 (PP2A) for binding to Axin1 upstream of β-catenin. Furthermore, SAPCD2 appeared to negatively regulate the transcription of Wnt target genes in both cultured cells and zebrafish. The co-localization of SAPCD2 puncta with that of Axin1 in the cytoplasm of intact HeLa cells as well as the reduction of PP2A/Axin1 complex formation as a function of increasing SAPCD2 expression reinforced the prediction that SAPCD2 modulates the Wnt/β-catenin pathway through outcompeting PP2A for direct interaction with Axin1 [85]. The apparent tumor-suppressive roles played by SAPCD2 in the early development of zebrafish presents an opportunity to explore the possibility of point mutations contributing to the transformation of SAPCD2 from an early tumor suppressor to a potent oncogene. Interestingly, another study demonstrated that SAPCD2 contributes to accelerated chromosomal segregation by interaction with the PP2A signaling network [87].

Endogenous and Exogenous Modulators of SAPCD2

Like most protein coding genes, SAPCD2 is modulated by endogenously produced microRNAs (miRNAs). However, the lack of homology across species in the SAPCD2 3'-untranslated region (3'-UTR) presents a challenge in identifying conserved binding sites and associated miRNAs that regulate its expression. Despite these challenges, one particular class of miRNA, denoted miR-29, has been found to repress SAPCD2 expression at both the post-transcriptional and post-translational levels. Specifically, miR-29a has been identified as an important direct regulator of SAPCD2 expression by targeting positions 213-219 of the SAPCD2 3'-UTR [73]. An inverse relationship between miR-29a and SAPCD2 expression has been observed in gastric cancer cell lines as well as gastric cancer tissue samples [73]. Furthermore, silencing of SAPCD2 by miR-29a in gastric cancer cell lines resulted in G_1 cell cycle phase arrest [73]. MiR-29a has likewise been identified as a tumor-suppressor in both lung and pancreatic cancer cell lines, where it functions to reduce the invasive potential and proliferation of these cells through mechanisms other than SAPCD2 repression [88]. The tumor suppressive function of miR-29a is further supported by its documented downregulation in several other types of solid tumors including neuroblastoma, sarcomas, and brain tumors [89]. Because miR-29a is a confirmed direct modulator of SAPCD2 expression and an evidence-supported tumor suppressor in solid tumors such as neuroblastoma, there emerges a possibility that SAPCD2 may be implicated in the development and progression of neuroblastoma.

Other ways to modulate endogenous SAPCD2 expression include long noncoding RNA (lncRNA). Like miR-29a, lncRNA PXN-AS1-L directly interacts with SAPCD2 mRNA in the 3'-UTR region [69]. However, LncRNA PXN-AS1-L functions to increase the expression of SAPCD2 at the mRNA and protein levels by preventing the binding of miRNA-AGO silencing complex, likely involving miR-29a, to the mRNA transcript [69]. PXN-AS1-L and miR-29a therefore appear to have competing functions in modulating SAPCD2 expression levels, where miR-29a decreases translation and PXN-AS1-L increases translation by blocking the RNA-induced silencing complex (RISC) formed between miR-29a and Argonaute-family proteins from binding to the mRNA transcript of SAPCD2. PXN-AS1-L and SAPCD2 expression have been found to be directly correlated and implicated in the proliferation, migration, and invasion of nasopharyngeal carcinoma (NPC) [69]. The expression level of PXN-AS1-L, and therefore SAPCD2, is negatively associated with mean overall survival of NPC patients [69].

Non-synonymous single nucleotide polymorphisms (SNPs) are characterized as single point mutations that alter the amino acid sequence of a protein. Specifically, non-synonymous SNPs within genes located on chromosome 9 are associated with various cancers, especially of the lung [90-92]. A single non-synonymous variant SNP identified in SAPCD2 has been discovered in five lung cancer samples, but not in normal lung mucosa samples [93]. These findings suggest that SAPCD2 may also be implicated in the tumorigenicity of lung cancer.

Other Disease States Associated with SAPCD2

In addition to the roles played by SAPCD2 in various types of neuroendocrine cancers, some evidence in favor of SAPCD2 contributing to other diseases has emerged. SAPCD2 may play an epigenetic role in the risk of cancer development in children born to mothers with high gestational BMI [94]. A high maternal BMI is predicted to alter the methylation patterns in infants and change genetic predispositions to cancer and other diseases prior to birth [94]. Interestingly, SAPCD2 expression has also been positively correlated with gastric mucosal inflammation and is enhanced by tumor necrosis factor (TNF)-α and *H. pylori* in a time-dependent manner [65]. Additionally, a group successfully retarded melanoma tumor growth in mice by vaccination with a pcDN3-SAPCD2 vector to elicit an anti-SAPCD2 specific immune response. This response was accompanied by increased levels of IFN-γ, perforin, and granzyme-B-producing $CD8^+$ T cells [95].

Overall, studies investigating the potential oncogenic function of SAPCD2 have recently extended beyond gastrointestinal cancers to include hepatocellular carcinoma and small cell carcinomas, such as those affecting the lung. It appears as though SAPCD2 may not only be important in determining the oncogenic pathway of gastric cancers, but of several neuroendocrine cancers. The apparent relevance of SAPCD2 expression in embryonic progenitors, neuroepithelial precursors, and neuroendocrine tumorigenesis presents an opportunity to explore its relevance in neuroblastoma. To the best of our knowledge, investigation of a possible connection between SAPCD2 and neuroblastoma has

not yet been attempted in the current literature.

RNA Interference

In 1997, revolutionary progress was made in biotechnology with the introduction of RNA interference (RNAi) by Andrew Z. Fire and Craig C. Mellow [96]. The introduction of synthetically produced double-stranded RNA (dsRNA) into eukaryotic organisms to interfere with the expression of endogenous genes has since become an integral part of understanding gene function and regulation patterns. Additionally, RNAi has been explored for its promising applications as a therapeutic tool in the development of novel drug free approaches to treating human diseases and heavily depends upon progress made towards identifying genetic targets in these disease pathways.

In eukaryotes, co-transcriptional and post-transcriptional gene modifications are achieved by two general classes of double-stranded regulatory RNAs, endogenous miRNA and exogenous short interfering RNA (siRNA) often introduced from viral sources. The production and processing of miRNA begins in the nucleus with primary miRNA (pri-miRNA) transcribed by RNA Polymerase II (Pol II) [97]. The nuclear pri-miRNA transcript is cleaved by the microprocessor complex, composed of a DiGeorge Snydrome Critical Region 8 (DGCR8) RNA-binding protein (RBP) and an RNase III family Drosha protein [98]. Following cytoplasmic export, precursor RNA (pre-miRNA) undergoes a series of processing reactions including cleavage by RNase III family Dicer protein for loading onto the RNA-induced silencing complex (RISC). The RISC loading

complex is composed of the dsRNA bound to Dicer, an Argonaute family protein, and a dsRBP and becomes activated following the ejection of one strand of silencing RNA. The remaining strand of RNA in the activated RISC is referred to as the guide strand and functions to direct sequence-specific target cleavage or translation inhibition [98].

The use of synthetically produced siRNA has gained popularity in studies aimed at understanding the function of particular genes in various human disease pathways. One of the most popular applications of siRNA-mediated knockdown of gene function is to guide research exploring the contributory roles of oncogenes in the initiation and progression of cancer. Identification of oncogenes in an important first step to developing novel anti-cancer drugs and is often followed by structural studies to determine the potential of the gene's DNA region, mRNA transcript, or protein translation product as druggable targets. However, unravelling the regulatory network of target oncogenes is often equally valuable in the development of novel anti-cancer therapies.

Regulatory RNAs in the research setting can be introduced into cells utilizing a variety of delivery systems. The advantages and disadvantages of each system must be carefully considered for the specific applications and treatment goals. Some of the significant challenges faced by RNAi delivery systems in the clinical setting include renal filtration, poor cellular uptake, entrapment by phagocytes, enzymatic degradation, off-target effects, extravasion, and immunogenicity [99, 100]. Some common delivery systems include lipid-based nanovectors, cyclodextrin-containing polymers, and dynamic

polyconjugates [100]. Of the available delivery systems, lipid-based nanovectors are among the most popular.

Hypothesis and Project Goals

The goal of this project was to investigate whether SAPCD2 possesses an oncogenic function when expressed beyond embryogenesis that contributes to poor prognosis in pediatric neuroblastoma. Our hypothesis is that SAPCD2 functions as an oncogene in neuroblastoma and contributes to disease progression and poor prognosis. Retrospective clinical investigations were conducted to identify whether higher expression levels of SAPCD2 are correlated with poor overall and recurrence free survival of neuroblastoma patients. Following this, *in vitro* investigations were conducted utilizing two independent human neuroblastoma cell lines to determine the effect of siRNA-mediated knockdown of SAPCD2 on malignant cell behavior. Quantitative reverse transcription PCR and western blotting were used to assess the efficacy of SAPCD2 knockdown at the mRNA and protein levels following transfection with a number of siRNAs. Once successful knockdown was confirmed, metabolic assays were used to quantitatively assess the effect of SAPCD2 knockdown on neuroblastoma cell viability. Because differentiation status is a major factor in staging tumor aggressiveness, the effect of SAPCD2 knockdown on neuroblastoma cell differentiation was assessed by evaluating morphological changes in response to transfection with siRNAs. Finally, clonogenic assays were utilized to assess the effect of siRNA-mediated knockdown of SAPCD2 on

the proliferative capacity of neuroblastoma cells.

II. MATERIALS AND METHODS

Materials

General reagents. Acrylamide/Bis-(29:1) (Cat #J63079) was obtained from Alfa Aesar (Wardhill, MA). 96-well PCR plates (Cat #4346906), high-capacity cDNA reverse transcription kit (Cat #4368813), and optical adhesive films (Cat #4311971) were purchased from Applied Biosystems (Foster City, CA). The BE(2)-C cell line (CRL-2268) was obtained from American Type Cell Culture (Manassas, VA). N,N,N',N'-Tetramethylethylenediamine (TEMED) (Cat #161-0800) was purchased from Bio-Rad (Hercules, CA). BLUEstain Protein Ladder (Cat #P007) was purchased from GoldBio (St. Louis, MO). 0.2 mL rainbow PCR tubes (Cat #A-1001-Z) were purchased from Light Labs (Redwood City, CA). 6X purple gel loading dye (Cat #B7024S) was obtained from New England Biolabs (Ipswich, MA). Tris (Cat #SC-3715B) was purchased from Santa Cruz Biotechnology (Dallas, TX). β-Mercaptoethanol (Cat #M6250), GAPDH primers **(Table 3)**, SAPCD2 primers **(Table 3)**, and sodium dodecyl sulfate (Cat #436143) were purchased from Sigma-Aldrich (St. Louis, MO). 2X SYBR Green qPCR reaction mix (Cat #K0221), thiazolyl blue tetrazolium bromide (Cat #158990010), isopropanol (Cat #A416-4), chloroform (Cat #15821-0010), TRIzol reagent (Cat #15596018), spectra multicolor broad range protein ladder (Cat #26634), Pierce BCA protein assay kit (Cat #23225), triton X-100 (Cat #AC422355000), tween 20 (Cat #23336-0010), Maxima SYBR Green/ROX qPCR 2X master mix (Cat #K0221), RNase*Zap* (Cat #AM9780), 1 Kb Plus DNA ladder (Cat #10787018), and dimethyl sulfoxide (Cat #BP231-1) were purchased

from Thermo Fisher Scientific (Waltham, MA). Glycine (Cat #97063-738) was purchased from VWR International (Radnor, PA).

Cell culture reagents. EquaFetal EFBS (Cat #EF-0500-A) was provided by Atlas Biologicals (Fort Collins, CO). DMEM/F-12 cell culture media (Cat #10-090-CV), 1X Dulbecco's phosphate buffered saline (DPBS) (Cat #21-031-CV), 1X 0.05% Trypsin (Cat #25-052-CI), 100 mm cell culture plates (Cat #430167), 60 mm cell culture plates (Cat #430166), Penicillin/Streptomycin (Cat #30-002-CI), and 96-well cell culture plates (Cat #3595) were obtained from Corning Incorporated (Corning, NY).

Western Blot Reagents. Gel electrophoresis rig (Cat #1658004EDU) and western blot transfer rig (Cat #1660828EDU) were obtained from Bio-Rad Laboratories (Herculues, CA). Resolving buffer (Cat #BP-90) and stacking buffer (Cat #BP-95) were purchased from Boston BioProducts (Ashland, MA). Primary anti-c9orf140 antibody (Cat #NBP1-91740) **(Table 5)** was provided by Novus Biologicals (Centennial, CO). Dry non-fat milk powder (Cat #M17200-1000.0) was purchased from Research Products International (Mt. Prospect, IL). Primary anti-Calnexin antibody (Cat #PA5-34754) **(Table 5)**, SuperSignal West Pico PLUS chemiluminescent substrate luminol/enhancer solution (Cat #1863097), SuperSignal West Pico PLUS chemiluminescent substrate stable peroxide solution (Cat #1863096), goat anti-rabbit IgG secondary Ab-HRP (Cat #31460), Pierce protease inhibitor mini tablets (EDTA-free, Cat #88266), and PVDF

transfer membrane 0.45 μM 26.5 cm (Cat #88518) were purchased from Thermo Fisher Scientific (Waltham, MA). 200 X 250 mm filter paper (Cat #10547922) was obtained from Whatman plc (Maidstone, UK).

Transfection reagents. SiRNAs 1 and 3 targeting SAPCD2 were purchased from Origene Technologies (Montgomery County, MD) **(Table 4)**. SiRNAs 131 (Cat #265184716) and 132 (Cat #265184719) targeting SAPCD2 **(Table 4)** were purchased from Integrated DNA Technologies (Coralville, IA). Lipofectamine RNAiMAX (Cat #56532) was obtained from Invitrogen (Carlsbad, CA).

Equipment. Inverted Trinocular Microscope 40X-800X (Cat #IN200TB) was purchased from Amscope (Irvine, CA). Allegra 6 centrifuge was purchased from Beckman Coulter (Brea, CA). ChemiDoc XRS+ Molecular Imager (Cat #1708265) was obtained from Bio-Rad Laboratories (Herculues, CA). Canoscan 9000F Mark II was provided by Canon (Ota, Tokyo, JP). Axyspin R refrigerated centrifuge (Cat #601-05-031) was purchased from Corning Incorporated (Corning, NY). IncucyteZOOM was purchased from Essen Bioscience (Ann Arbor, MI). SpectraMAX 190 Spectrophotometer (Cat #254428481441) was obtained from Molecular Devices LLC (San Jose, CA). Nanodrop 2000 (Cat #ND-2000), Fisher Vortex Genie 2 (Cat #12.812), Dry Bath Incubator, coverslides (Cat #0267110), 7500 Fast Real-Time PCR System (Cat #4351106), Sorvall Legend X1R (Cat #75004261), and Forma^{TM} Series 3 Water Jacketed CO_2 Incubator

(Cat #4110) were purchased from Thermo Fisher Scientific (Waltham, MA). CK Olympus Tokyo Inverted Microscope and Neubauer Improved Hemocytometer (Cat #1103) were purchased from Olympus Corporation (Shinjuku, Tokyo, JP). Hermle MR-2 Tabletop Centrifuge was purchased from Labnet International (Edison, NJ).

Software. SoftMaxPro 5.4.1 purchased from Molecular Devices LLC (San Jose, CA). High Resolution Melt (HRM) Software v2.0 (Cat #4397808) and Nanodrop 2000/2000c Operating Software v2.6 were obtained from Thermo Fischer Scientific (Waltham, MA). Image Lab™ Software (Cat #1708265) was purchased from Bio-Rad Laboratories (Hercules, CA).

Table 3. Primers used in this thesis work

Target	Sequence	Description
SAPCD2	CAGACCATCCTCATGCTGAAG	P42.3-RTPCR-F
	TTAATGAGCGCCGACTTCTC	P42.3-RTPCR-R
GAPDH	GAAGGTGAAGGTCGGAGTC	h-GAPDH-F
	GAAGATGGTGATGGGATTTC	h-GAPDH-R

Table 4. SiRNAs used in this thesis work

siRNA	Sequence	Company
Origene siR-1	CAGACCATCCTCATGCTGAAG	Origene Technologies
Origene siR-3	TTAATGAGCGCCGACTTCTC	
IDT siR-131	GAAGGTGAAGGTCGGAGTC	Integrated DNA Technologies
IDT siR-132	GAAGATGGTGATGGGATTTC	

Table 5. Antibodies used in this thesis work

Antigen	Sequence	Position
Calnexin	KEEEEEKEEEKDKGDEEEEGEEKLEEKQKSDAEED GGTVSQEEEDRKPKAEEDEILNRSPRNRKPRRE	525-592
SAPCD2	LGQSRASADFGAAGSPRPLGRL	234-301

Methods

Neuroblastoma Patient Genomic Analysis. Patient analysis was conducted utilizing the free online R2: Genomics Analysis and Visualization Platform. The tumor neuroblastoma dataset for analysis was selected and the type of analysis was set to “view a gene”. The SAPCD2 gene was manually inserted, relative sample filters were applied, and data was 2log transformed. Kaplan-Meyer curves were automatically generated, and expression cutoffs were standardized by manual selection. Expression values were sorted in Microsoft Excel and analyzed with GraphPad Prism 8.0.

Cell Culture. BE(2)-C cells were grown in 100 mm cell culture dishes with 12.0 mL of DMEM/F-12 cell culture media supplemented with 10% (v/v) EquaFetal Bovine Serum (EFBS) and 1% (v/v) penicillin/streptomycin and incubated at biological conditions (37^{o}C, 5.1% CO_2, 75% RH). Cells were passaged approximately every 4-5 days or at 85% confluency. Passaging was achieved by the sterile removal of old growth media followed by a brief rinsing with phosphate-buffered saline (PBS) and the addition of 1.0 mL 0.05% Trypsin for five minutes. Following adequate detachment and separation by pipetting,

trypsin was neutralized with full DMEM/F-12 cell culture media (supplemented with 10% EFBS and 1% P/S) and cells were centrifuged at 3,000 rpm for 5 minutes. The resulting cell pellets were resuspended in the appropriate media for counting and downstream use in experiments.

MTT Assay. The effect of SAPCD2 depletion on neuroblastoma cell survival was assessed by MTT colorimetric assays **(Figure 4)**. In this assay, the soluble chromophore 3-(4,5-dimethylthiazol-2-yl)-2,5-diphenyltetrazoliumbromide (MTT) is reduced by NADH-dependent reductase enzymes in live, metabolizing cells to a crystallized formazan solute with a vivid purple color. The formazan crystals are subjected to spectrophotometric analysis and provide a quantitative

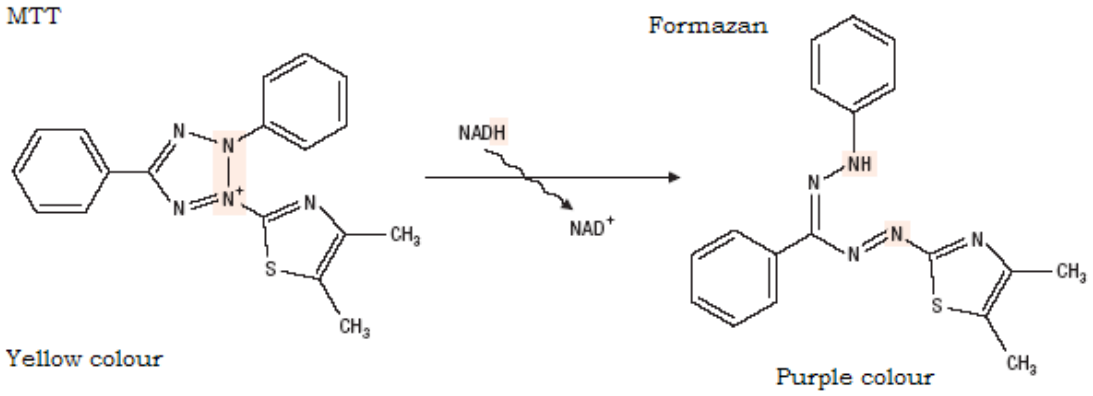

Figure 4. MTT Cell Viability Assay. Neuroblastoma cells are transfected with siRNAs and grown at physiological conditions for four days. On day five, soluble MTT reagent is diluted in cell growth media and applied to the cells for 1-4 hours. Following incubation, insoluble formazan crystals resulting from the above metabolic reaction in live cells are measured spectrophotometrically at 570 nm with a reference wavelength of 630 nm. Absorbance values provide a direct measurement of living cells in the sample. Figure reproduced from [101].

assessment of cell viability. MTT working solution was homemade by dissolving 5.0 g of thiazolyl blue tetrazolium bromide in ethanol and diluting with PBS to a

final concentration of 2.5 mg/mL. The resulting solution was mixed with DMEM/F-12 cell culture media (7.5% v/v) and stored at 4ºC away from light. For treatment of 96-well plates, 50 μL of homemade MTT working solution was added to each well and incubated at 37ºC for 1-4 hours. The plates were centrifuged at 2,000 rcf for 5 minutes and the MTT media was discarded. Remaining crystallized MTT reagent was solubilized in 50 μL DMSO and incubated at 37.5ºC for five minutes. The plates were read with a SpectraMAX 190 spectrophotometer and data was collected using SoftMaxPro 5.4.1. Data analysis was conducted using Microsoft Excel and GraphPad Prism.

Reverse Transfection with siRNA. RNAiMAX dilutions were prepared by mixing enough transfection reagent for 0.3 μL RNAiMAX per well with plain DMEM/F-12 cell culture media (not supplemented with EFBS or P/S) to a total volume of 15 μL per well. Indicated siRNAs were plated and conjugated with 15 μL of Lipofectamine RNAiMAX dilution per well in 96-well plates. The RNAiMAX-siRNA complexes were mixed by gentle tapping and allowed to form micelles at room temperature for five minutes before the introduction of cells diluted in DMEM/F-12 cell culture media supplemented with 10% (v/v) EFBS to each well in the specified amounts. On day two, complete DMEM/F-12 culture media (supplemented with 10% EFBS and 1% P/S) was added to each well. The transfections were incubated at 37ºC for 4-5 days before completion of metabolic and cell viability assays. Images were obtained utilizing the IncucyteZOOM equipment and associated software and cell phenotype was assessed as a

measurement of differentiation status.

Forward Transfection with siRNA. On day one, enough cells were added to 60 mm cell culture plates to reach approximately 30% confluency within 24 hours. On day two, RNAiMAX-siRNA complexes were prepared by mixing 100 μL of siRNA diluted in molecular biology grade water with 100 μL RNAiMAX diluted in plain DMEM/F-12 cell culture media without EFBS or P/S supplementation to a final concentration of 3 μL/mL of total transfection volume. The complexes were mixed and allowed to form micelles at room temperature for 5 minutes. In the meantime, the cell culture media was removed from each plate and cells were rinsed with plain DMEM/F-12 culture media. 800 μL of plain DMEM/F-12 cell culture media was added to each plate and 200 μL of RNAiMAX/siRNA complex was added in a dropwise fashion with swirling. The cells were incubated at 37℃ for two hours before the addition of 3 mL of full DMEM/F-12 cell culture media supplemented with 10% (v/v) EFBS and 1% (v/v) P/S. The transfected cells were allowed to grow at 37℃ for 48-72 hours before collection and use in downstream applications.

Fast forward Transfection with siRNA. Cells were passaged according to general procedure and resuspended in 638 μL of plain DMEM/F-12 culture media to the final concentration noted in each experiment. In a separate set of 1.5 mL microcentrifuge tubes, the amount of siRNA necessary for a final concentration of 20 nM in 700 μL was diluted with molecular biology grade water

to a volume of 34 μL. In an additional set of 1.5 mL microcentrifuge tubes, 2.31 μL of Lipofectamine RNAiMAX was mixed with 31 μL of plain DMEM/F-12 cell culture media for each siRNA treatment. 31 μL of each siRNA dilution was mixed with 31 μL of each RNAiMAX dilution in a third set of 1.5 mL microcentrifuge tubes and incubated at room temperature for 5 minutes. 638 μL of cell suspension was added to each tube and rocked slowly for 1-2 hours at room temperature. Following transfection, each cell suspension was mixed with DMEM/F-12 cell culture media supplemented with 10% (v/v) EFBS and 1% (v/v) P/S for use in downstream applications.

Imaging. Cells were plated and treated in 96-well plates prior to imaging in an IncucyteZOOM Live Cell Imaging System under 20X magnification at specified time points. Resulting images were subject to cell body and neurite colorimetric detection by the IncucyteZOOM software. Processing definitions were manually optimized to detect fine neurite outgrowth. Cell confluency was used to estimate proliferation throughout the duration of experiments.

Colony Formation Assay. Cells were transfected with siRNAs according to the fast forward transfection protocol and plated onto 10 mm cell culture dishes in specified amounts. The cells were incubated in DMEM/F-12 culture media supplemented with 10% (v/v) EFBS and 1% (v/v) penicillin/streptomycin at 37^{o}C, 5.1% CO_2, and 75% RH for 1-3 weeks or until colonies of adherent cells were visible from the bottom of the plates. The cells were rinsed with 1X

phosphate buffered saline (PBS), stained with 0.5% crystal violet for 20 minutes, rinsed with 1X PBS again, and allowed to air dry at room temperature for 24 hours. Plates were scanned using a CanoScan 9000F Mark II and colony size and number were analyzed using the ImageJ software.

Cell Lysate Collection. Following 24-72hr treatment with specified siRNAs, cells were rinsed with 1X PBS and incubated on ice for 3 minutes. Adherent cells were removed from the plate by manual scraping in the presence of 100 μL ice cold lysis buffer [98.9% (v/v) dH_2O, 0.3% (w/v) Tris 25 nM, 0.02% (w/v) KCl 2.7 nM, 0.8% (w/v) NaCl 137 mM] and incubated on ice for 10 minutes. Cell debris was centrifuged at 14,000 rpm for 5 minutes and the supernatant was transferred to a new set of Eppendorf tubes. The total volume of collected supernatant was recorded for downstream calculations. The supernatant was mixed in a 75:25 ratio with 5X protein loading buffer [16% (v/v) 2 M Tris-HCl, pH 6.8; 21.5% (v/v) dH_2O, 50% (v/v) glycerol, 5% (w/v) bromophenol blue, 10% (w/v) SDS, 12.5% (v/v) 2-mercaptoethanol] and heat-denatured at 95^{o}C for 5 minutes. Cell lysates were stored at -20^{o}C.

BCA Assay. 12.5 μL of BSA standard was added to each well of a 96-well plate (working range = 20-2,000 μg /mL) and 5 μL of sample protein was added to each well in the row below the standards. BCA Reagents A and B were mixed at a ratio of 50:1 and 0.2 mL of the resulting solution was added to each well. The plate was covered and incubated at 37^{o}C for 30 minutes and absorbance

was measured at 562 nm.

SDS-PAGE Gel Preparation. 8% SDS resolving gels were prepared with 54% (v/v) sterile deionized water, 25% (v/v) tris buffer [1.5 M tris, 0.4% SDS pH 8.8], 20% (v/v) 40% acrylamide/bis, 0.1% (v/v) 10% APS, and 0.01% (v/v) TEMED. The liquid gel mixture was vortexed briefly and poured into a Mini-PROTEAN Tetra handcast system. A small volume of 75% ethanol was applied to the surface of the mixture. The gel was allowed to harden at room temperature for approximately 15 minutes and the 75% ethanol was removed. 4% SDS stacking gels were prepared with 64% (v/v) sterile deionized water, 25% (v/v) tris buffer [0.5 M tris, 0.4% SDS, pH 6.8], 10% (v/v) 40% acrylamide/bis, 1% (v/v) 10% APS, and 0.01% (v/v) TEMED. The liquid mixture was vortexed briefly and added to the polymerized resolving gel. 10-well combs were immediately positioned in each cast and gels were allowed to harden at room temperature for approximately 15 minutes.

SDS-PAGE. SDS-PAGE gels were homemade according to the gel preparation procedure. Two gels were assembled in the gel running cassette with lower edges facing in. The chamber was filled to the maximum volume with 1X running buffer [98.3% (v/v) dH_2O, 0.3% (w/v) Tris, 1.4% (w/v) glycine, 0.01% (w/v) SDS] and 10-well combs were removed. Samples were prepared for running by mixing thoroughly with enough 1X protein loading buffer [4% (v/v) 2 M Tris-HCl, pH 6.8; 76.6% (v/v) dH_2O, 12.5% (v/v) glycerol, 1.25% (w/v)

bromophenol blue, 2.5% (w/v) SDS, 3.1% (v/v) 2-mercaptoethanol] to load a minimum volume of 10 μL into each well, if required. 15 μL of Spectra multicolor broad range protein ladder was added to lane one of each gel and samples were loaded according to the specified protein amounts. SDS-PAGE gels were run at 100V for approximately 80 minutes.

Transfer to Nitrocellulose Membrane. 1X transfer buffer [98.3% (v/v) dH_2O, 0.3% (w/v) 25 nM Tris, 1.4% (w/v) glycine 192 nM] was pre-chilled at 4℃ prior to use. A 3” x 3.8” section of PVDF membrane was immersed in 100% methanol with rocking for 3 minutes then soaked in deionized water with rocking for 5-10 minutes. Within the transfer cassette, sandwiches were made by stacking a sponge soaked in cold 1X transfer buffer, filter paper soaked in cold 1X transfer buffer, SDS-PAGE gel, soaked PVDF membrane, filter paper soaked in cold 1X transfer buffer, and an additional sponge soaked in cold 1X transfer buffer. Even contact between SDS-PAGE gel and PVDF transfer membrane was established by rolling across the surface of the membrane with a falcon tube. The transfer sandwiches were assembled in the cassette with an ice pack, and the chamber was filled with cold 1X transfer buffer. The entire apparatus was placed on ice and the transfer was completed at 200 mAmps for 2 hours.

Blotting Nitrocellulose Membranes. Following transfer of proteins onto the nitrocellulose membrane, a small notch was made in the upper left-hand corner of the membrane to indicate which side of the membrane was in direct

contact with the SDS-PAGE gel during transfer. The membrane was rinsed in homemade blocking buffer [95% (v/v) 1X TBS buffer, 5% (w/v) dry non-fat milk powder, 0.05% (v/v) Tween 20] and submersed in fresh blocking buffer for 48 hours at 4℃. Following removal of blocking buffer, the membrane was briefly rinsed with 1X TBST buffer [90% (v/v) dH_2O, 10% (v/v) 10x TBS, 0.05% (v/v) Tween 20] and the appropriate primary antibody was applied to the gel side of the membrane at a 1:1,000 ratio in 1X TBST buffer. The membrane was incubated with primary antibody overnight, and on the following day was washed three times for ten minutes each in 1X TBST buffer with gentle rocking. HRP-conjugated secondary antibody was applied at a 1:20,000 ratio in TBST buffer for one hour with gentle rocking and the three ten-minute wash steps in TBST were repeated. Chemiluminescent substrate was prepared by mixing SuperSignal™ West Pico PLUS enhancer and stable peroxide solutions in equal parts and applied to the membrane for 5-10 minutes. Membranes were imaged with a Bio-Rad ChemiDOC XRS+ Imaging system.

Extracting Total RNA Utilizing TRIzol. Following 48-72 hour transfection with siRNAs in 60 mm dishes, growth media was removed by sterile suctioning and cells were rinsed with 1X Dulbecco's phosphate-buffered saline (DPBS). 3.0 mL of TRIzol reagent was added to each 60 mm dish and cells were lysed by vigorous pipetting. Homogenates were transferred to 1.5 mL microcentrifuge tubes and incubated at room temperature for five minutes to facilitate complete dissociation of nucleoprotein complexes. 200 μL of chloroform per 1.0 mL of

TRIzol was added to each mixture, and the mixtures were vigorously shook by hand for 15 seconds and incubated at room temperature for 2 minutes. The samples were centrifuged at 12,000 rcf for 15 minutes at 4℃ and the RNA-containing aqueous phase of each sample was carefully removed and transferred into a new set of tubes. 500 μL of 100% isopropanol was added to each aqueous phase per 1.0 mL of TRIzol and the samples were incubated at room temperature for 10 minutes prior to centrifugation at 12,000 rcf for 10 minutes at 4℃. The resulting supernatant was removed, and the remaining RNA pellets were washed with 1.0 mL of 75% ethanol per 1.0 mL of TRIzol. The washes were centrifuged at 7,500 rcf for 5 minutes at 4℃ and the supernatant was discarded. The RNA pellets were air dried for 10 minutes at room temperature and resuspended in nuclease-free water. RNA concentration and purity were determined using the Nanodrop 2000 instrument.

Agarose Gel Electrophoresis to assess RNA purity and integrity.

Prior to gel casting, all materials and surfaces were treated with a generous amount of commercial RNase inhibitor RNase*ZAP*, rinsed with deionized water, and allowed to dry. 1.8% agarose gels were prepared by adding 0.72 grams of dry agarose powder to 40 mL of 1X TAE buffer and heating to fully dissolve agarose particulates. 2.0 μL of ethidium bromide was added to the molten agarose mixture and combined by swirling. The gel was poured into a mold with a 15-well comb and allowed to solidify for 20 minutes. Following complete polymerization, the gel was arranged in a horizontal electrophoresis cell and

submerged in 1X TAE buffer. 300 μg of each RNA sample was mixed with 6X purple DNA loading dye in a volumetric ratio of 5:1 and loaded into each well. Electrophoresis was carried out at 100 V for approximately 40 minutes. The gels were rinsed with deionized water and imaged with a Bio-Rad ChemiDoc XRS+ imaging system.

Reverse Transcription. Reverse transcription was carried out with the use of the high-capacity cDNA reverse transcription kit from Thermo Scientific. 2X RT master mix was prepared for each 20 μL reaction using the kit components with unit volumes specified in **Table 6**. 2 μg of each purified RNA sample was diluted in molecular biology grade water to a final volume of 10 μL and combined with 10 μL of prepared 2X master mix in PCR tubes. The samples were incubated overnight at 37℃ to allow completion of the reverse transcription reaction. Resulting cDNA concentrations were equal to 100 ng/μL. Samples were stored at -20℃ prior to use in PCR experiments.

Table 6. 2X RT Master Mix Components

Component	**Unit Volume (μL)**
10X RT Buffer	2
dNTP Mix (100 mM)	0.8
10X Random Primers	2
Reverse Transcriptase	1
RNase Inhibitor	0.5
Nuclease-free H_2O	3.7
Total	10

Real-Time PCR. 20X PCR primer mixes were prepared for each set of primers by mixing 2.0 μL of each forward and reverse primer at stock concentrations of 100 μM with 16.0 μL of nuclease-free water. All cDNA samples were diluted in molecular biology grade water to 2.5 ng/μL for use in qPCR. SYBR green master mixes [10% (v/v) 20X primers, 90% (v/v) commercial 2X SYBR green mix] were prepared for each set of primers. 2.0 μL of cDNA was added to each well of a 96-well PCR reaction plate followed by 3.0 μL of SYBR green master mix for a total reaction volume of 5.0 μL and 5.0 ng of total template cDNA. Each reaction was mixed by gentle tapping and the 96-well plate was covered with an optical adhesive film. The plate was spun down in a salad spinner affixed with a 96-well plate holder secured to the interior chamber with zip ties. The real-time PCR reactions were carried out in an ABI 7500 fast real-time PCR system. The type of experiment run in the corresponding software was

"Quantitation-Comparative Ct (ΔΔCt)" and targets were defined in the plate setup section. Targets and samples were assigned to each well and the run method graph was populated with the PCR reaction conditions in **Table 7**. Fluorescence detection was initiated at the extension step with AutoDelta enabled.

Measuring RNA Concentration with Nanodrop 2000. Prior to measuring sample concentrations, routine wavelength verification was automatically initiated by the Nanodrop 2000 instrument. "Nucleic Acid" was selected as the application on the program home screen, and "RNA" was selected from the dropdown box. The sample platform and lever arm were thoroughly cleansed with a kimwipe dampened with deionized water, and 1.0 μL of plain molecular biology grade water was measured to blank the instrument. A 1.0 μL sample of each RNA was pipetted onto the sample platform and measured in triplicates, and the instrument was wiped dry with a kimwipe between each measurement. Sample concentrations, A_{260}/A_{280}, and A_{260}/A_{230} ratios were recorded for each RNA samples. The sample purity was considered acceptable for downstream applications when the A_{260}/A_{280} ratio exceeded 1.95.

Table 7. Real-Time PCR Reaction Conditions

Step	Temperature	Time	
UDG Pre-treatment	50℃	2 min	
Initial Denaturation	95℃	10 min	
Denaturation	95℃	15 sec	X 40 cycles
Annealing	60℃	30 sec	
Extension	72℃	30 sec	

Agarose Gel Imaging. The integrity of total RNA extracted from cells was assessed by gel electrophoresis and imaging with a Bio-Rad ChemiDOC XRS+ instrument. When prompted by the software to select a new protocol, “nucleic acid gel” was selected. Under protocol setup, the application was set to “Ethidium Bromide” and the filter on the imager was manually set at position 1. The default settings were maintained for the imaging area, and image exposure was set to automatic to optimize for intense bands. Under display options, “highlight saturated pixels” was unselected. After adjusting the gel for optimal positioning, the imaging was initiated by selecting “run protocol”. Resulting images were exported as 600 dpi TIFF files.

Western Blot Imaging. Following application of chemiluminescent substrate, western blot membranes were imaged with a Bio-Rad ChemiDOC XRS+ instrument. When prompted by the software to select a new protocol, “blots” was selected. Under protocol setup, the application was set to “Chemi Hi Resolution” and the filter on the imager was manually set to no filter. The default settings were maintained for the imaging area, and the signal accumulation mode was setup manually as 30 images over the span of 90 seconds. Under display options, “highlight saturated pixels” was unselected. After adjusting the PVDF membrane for optimal positioning, the imaging was initiated by selecting “run protocol”. Resulting images were exported as 600 dpi TIFF files.

III. RESULTS

The first step in investigating the oncogenic potential of a novel gene is determining whether higher expression levels of the relevant gene is correlated with poor patient prognosis, which may be measured as the overall length of survival following treatment or the length of survival following treatment without recurrence or return of disease (event-free survival). To do this, we utilized a free online genomic database called R2 that is publicly accessible through the web link https://hgserver1.amc.nl/cgi-bin/r2/main.cgi. Within this program, results can be filtered by cancer type, patient cohort, and gene expression. For this study, “tumor” was selected as the category and “neuroblastoma” was selected as the tissue or tumor of interest. Three independent groups of patients, totaling more than 1,200 patients, were evaluated for trends in prognosis as a function of SAPCD2 expression level. While analyzing the oncogenic potential of a gene utilizing this method is limited by the reductionist nature of assessing the effect of a single gene on a disease that involves vast networks of overlapping cellular events, it serves the purpose of providing a future direction for *in vitro* exploration.

Following our retrospective clinical investigation, we determined that the oncogenic potential of SAPCD2 warrants further analysis *in vitro*. To do this, we transfected two independent human neuroblastoma cell lines with a series of siRNAs targeting different regions of the SAPCD2 mRNA transcript. In order to validate successful knockdown at the mRNA and protein levels, we conducted quantitative reverse transcription PCR and western blotting experiments which

confirmed knockdown through multiple replicates. Our next step was then to determine the effect of siRNA-mediated knockdown of SAPCD2 on neuroblastoma cell survival, differentiation, and proliferation. To achieve this, we utilized a metabolic assay to quantify the relative number of live cells remaining four days after transfection with siRNAs. Differentiation status was measured qualitatively by observing morphological changes in response to SAPCD2 knockdown, and proliferative capacity was assessed by measuring the ability of neuroblastoma cells seeded at very low densities to form colonies over a period of approximately two weeks.

Retrospective Clinical Investigation Results

Within the R2 genomics analysis and visualization platform, the first patient cohort analyzed was Kocak 649 (platform ag44kcwolf), representing a single dataset of microarray expression data from 649 neuroblastoma patients under the “tumor neuroblastoma” analysis bin. The type of analysis was set to “view a gene”, and SAPCD2 was entered in the text box. Kaplan-Meier survival curves were generated for overall and event-free survival probability over a period of several months. Within the Kocak 649 cohort, incomplete survival data for 173 patients was recorded, and these patients were excluded from the Kaplan-Meier survival analysis. Within the overall patient population, there exists a significant difference in both the overall and event-free survival probabilities in patients with high SAPCD2 expression levels compared to those with low expression levels **(Figure 5A-B)**. Furthermore, there is a significant difference in

the SAPCD2 mRNA expression levels between the high and low expression groups **(Figure 5C)**. Because large groups of patients will naturally fall along a continuum of expression levels for a single gene, there is rarely a distinctive gap in expression level within the group that guides cutoff and organization into high and low expression groups. Instead, high and low expression groups were defined by first ranking the SAPCD2 expression level in all 476 patients from low

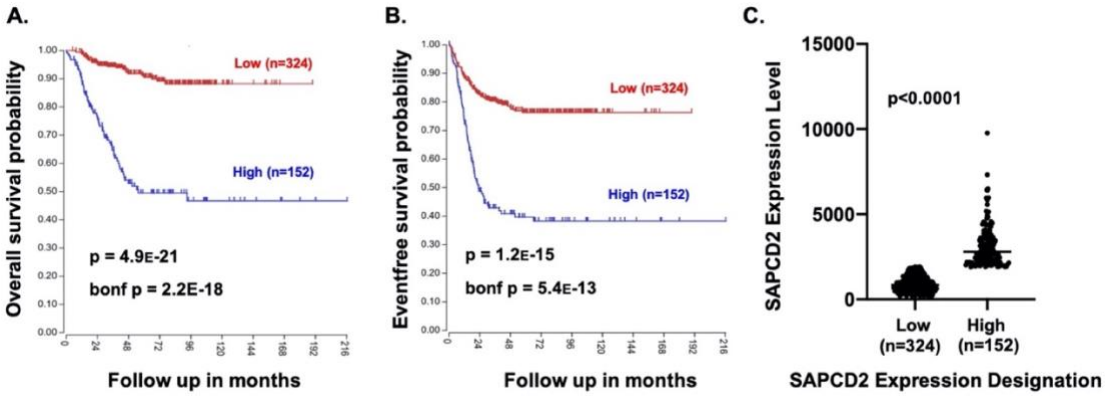

Figure 5. Kaplan-Meier Survival Analysis of Neuroblastoma Patients Expressing SAPCD2 in the Kocak Dataset. Patients were separated into two groups based on tumor SAPCD2 mRNA expression level (high and low) determined by an optimal expression level cutoff that resulted in the most significant difference between expression groups. Corresponding survival data was collected over a period of 216 months. **A**, Overall survival probability of neuroblastoma patients expressing low (red line) and high (blue line) mRNA levels of SAPCD2. The number of patients in each expression group is indicated in parentheses. **B**, Event-free survival probability of neuroblastoma patients expressing low (red line) and high (blue line) mRNA levels of SAPCD2. The number of patients in each expression group is indicated in parentheses. **C**, Expression cutoffs defining each SAPCD2 expression group. 173 samples lacked complete survival data and were excluded from the analysis. The Bonferroni p value (bonf p) represents a statistical correction for multiple comparisons and is a stricter analysis of the statistical significance.

to high and then by making incremental cutoffs separating the two groups at each individual expression level. The expression level cutoff that resulted in the most statistically significant difference between the two groups was utilized as

the expression level cutoff that defined the low and high expression groups. As a natural consequence of analyzing microarray expression data from several hundred patients whose expression levels are evenly distributed along a continuum, some overlap between the patients in the lower bounds of the high expression group and the patients in the upper bounds of the low expression group is expected.

In statistics, type I errors occur when the null hypothesis is incorrectly rejected, yielding an incorrect result that is often referred to as a “false positive”. The type I error rate often increases significantly when multiple hypotheses are being tested simultaneously, which obscures correct analysis of the dataset [102]. The family-wise error rate (FWER) is defined as the probability of a type I error occurring and increases substantially with an increasing number of simultaneous hypotheses **(Equation 1)**:

$$FWER = 1 - (1 - \alpha)^m \qquad \textbf{Equation 1}$$

Where α is the alpha level and m is the number of tests.

This phenomenon is commonly referred to as the multiple comparisons problem. Its effects can be reduced by adjusting the error rate to an appropriate level, which often results in a rise of type II errors in which the test fails to reject the null hypothesis [102]. A high proportion of type II errors, however, decreases statistical power. In order to control the type I error rate while still balancing statistical power, one of several multiple comparisons tests (MCTs) must be

applied [102]. The Bonferroni correction is one example of a MCT and is widely utilized due to its simplicity in understanding and application **(Equation 2)**:

$$Bonferroni\ corrected\ \alpha = \frac{\alpha}{k} \qquad \textbf{Equation 2}$$

Where α is the alpha level and k is the number of tests.

The resulting p value obtained following a Bonferroni correction is abbreviated bonf p and is indicated in each figure. Because MYCN is an important factor in classifying disease aggressiveness and risk group stratification in neuroblastoma [103, 104], the effect of SAPCD2 expression level within both MYCN amplified and non-MYCN amplified neuroblastoma tumors was also investigated to determine whether the oncogenic effect of SAPCD2 exists independently of MYCN amplification status. The same Kocak 649 dataset was evaluated with the addition of MYCN amplification status as a track, which separates the patient data shown in **Figure 5** into MYCN amplified **(Figure 6)** and non-MYCN amplified **(Figure 7)** groups. In these groups, the SAPCD2 mRNA expression cutoffs were determined as previously described.

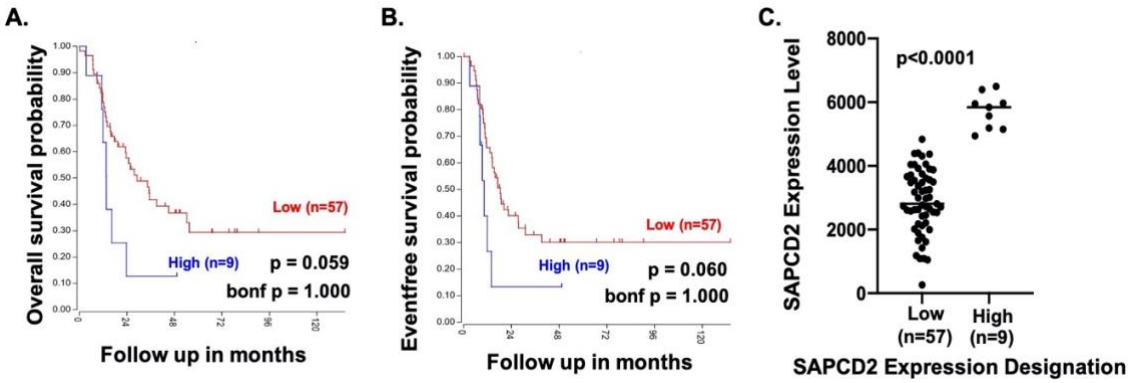

Figure 6. Kaplan-Meier Survival Analysis of MYCN Amplified Neuroblastoma Patients Expressing SAPCD2 in the Kocak Dataset. Neuroblastoma patients with MYCN amplified tumors were separated into two groups based on tumor SAPCD2 mRNA expression level (high and low) and corresponding survival data was collected over a period of 120 months. **A**, Overall survival probability of neuroblastoma patients with MYCN amplified tumors expressing low (red line) and high (blue line) levels of SAPCD2. The number of patients in each expression group is indicated in parentheses. **B**, Event-free survival probability of neuroblastoma patients with MYCN amplified tumors expressing low (red line) and high (blue line) levels of SAPCD2. The number of patients in each expression group is indicated in parentheses. **C**, Expression cutoffs defining each SAPCD2 expression group.

The results indicate that high levels of SAPCD2 mRNA are correlated with poor overall and event-free survival in high-risk neuroblastoma patients with MYCN amplified tumors, although unlike in the overall patient population, the effect did not reach statistical significance. This is likely due to the small sample size corresponding to both MYCN amplified patients compared to the overall patient population and only nine patients being included in the SAPCD2 high expression group. Furthermore, all nine patients within the high SAPCD2 expression group perished within 48 months, which may also complicate statistical interpretation. Nonetheless, the effect of SAPCD2 expression on survival probability appears qualitatively evident. In the non-MYCN amplified

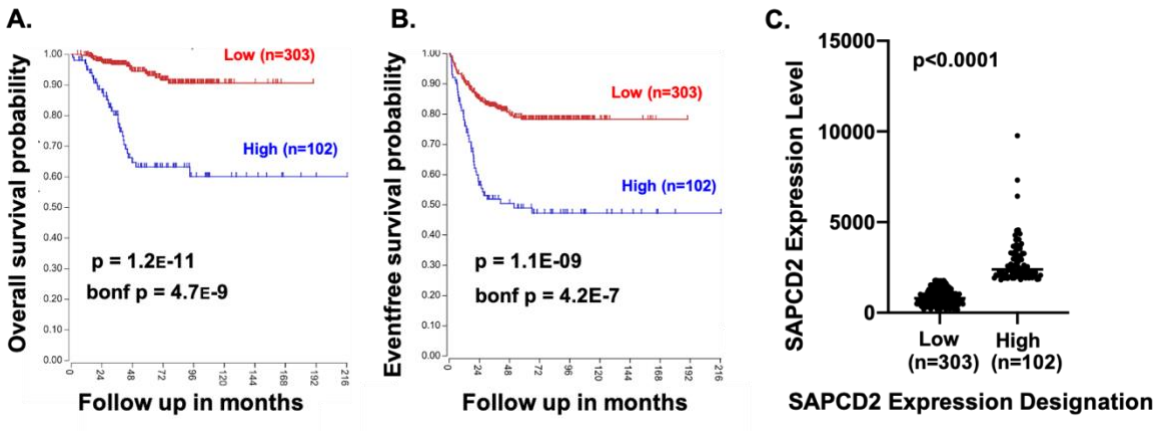

Figure 7. Kaplan-Meier Survival Analysis of non-MYCN Amplified Neuroblastoma Patients Expressing SAPCD2 in the Kocak Dataset. Neuroblastoma patients with MYCN-amplified tumors were separated into two groups based on tumor SAPCD2 mRNA level and the corresponding survival data was collected over a period of 216 months. **A**, Overall survival probability of non-MYCN amplified neuroblastoma patients expressing low (red line) and high (blue line) tumor SAPCD2 levels. The number of patients in each expression group is indicated in parentheses. **B**, Event-free survival probability of non-MYCN amplified neuroblastoma patients expressing low (red line) and high (blue line) tumor SAPCD2 levels. The number of patients in each expression group is indicated in parentheses. **C**, Expression cutoffs defining each SAPCD2 expression group.

patient population, high SAPCD2 expression levels are significantly correlated with a reduction in both overall and event-free survival probabilities **(Figure 7)** and corroborates the results described in **Figure 5**. Unlike the small patient population in **Figure 6**, the patient population in the non-MYCN amplified tumor group displays statistical significance between the survival probabilities of patients whose tumors express high and low levels of SAPCD2.

Next, we sought to investigate a second neuroblastoma patient cohort in order to validate the results obtained in the first dataset. The second cohort analyzed was SEQC 498 (platform ag44kcwolf), representing a single dataset of microarray expression data from 498 neuroblastoma patients under the “tumor neuroblastoma” analysis bin. Like the first patient cohort, the effect of tumor

SAPCD2 expression levels on overall and event-free survival probability were analyzed within the overall patient population as well as within patient populations with MYCN amplified and non-MYCN amplified tumors. In the overall patient population, there exists a significant difference between the survival probabilities of patients whose tumors express high levels of SAPCD2 compared to those expressing a low level, where a higher expression level of SAPCD2 is correlated with a significant reduction in both overall and event-free survival probability **(Figure 8A-B)**. Likewise, there exists a significant difference between the mRNA expression levels of SAPCD2 in the high and low expression groups **(Figure 8C)**. The effect of SAPCD2 expression level on survival probability was also investigated within the MYCN amplified patient cohort **(Figure 9)** and was found to be consistent with conclusions made in the Kocak dataset. Although a difference between the survival probabilities of each group appears evident, the relationship did not reach statistical significance following Bonferroni correction. However, unlike in the previous dataset, the raw p values for both overall and event-free survival probabilities suggest a statistically notable difference for the high and low expression groups which is abolished after the Bonferroni correction is applied. Like in the Kocak 649 patient cohort, the statistical power is vastly limited in the SEQC 498 dataset due to an extraordinarily small sample size of patients with high SAPCD2 expression within the MYCN amplified group. The correlation between high tumor SAPCD2 expression and poor survival probability

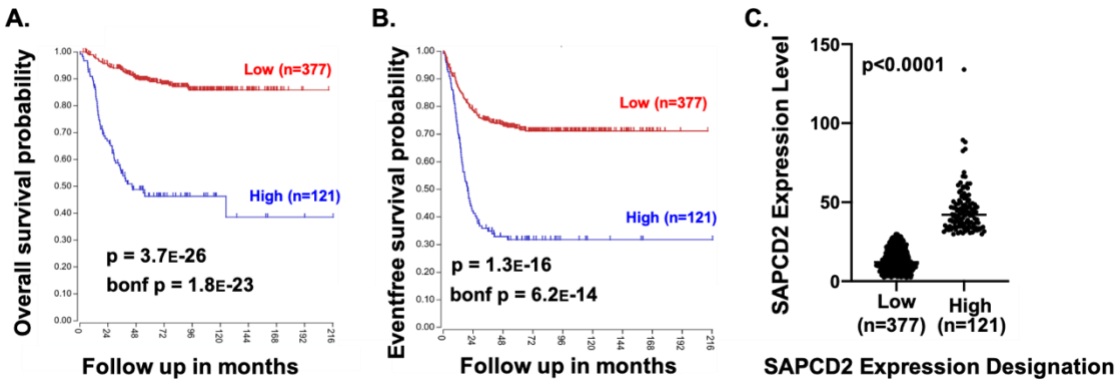

Figure 8. Kaplan-Meier Survival Analysis of Neuroblastoma Patients Expressing SAPCD2 in the SEQC Dataset. The general population of neuroblastoma patients within the SEQC498 dataset were separated into two groups based on tumor SAPCD2 mRNA level (high and low) and the resulting survival data was collected over a period of 216 months. **A**, Probability of overall survival for neuroblastoma patients expressing low (red line) and high (blue line) mRNA level of SAPCD2. **B**, Probability of event-free survival for neuroblastoma patients expressing low (red line) and high (blue line) mRNA levels of SAPCD2. The number of patients in each expression group is indicated in parentheses. **C**, Expression cutoffs defining each SAPCD2 expression group.

may still be recognized despite the lack of statistical significance in the MYCN amplified population, since the validity of the statistical test can be reasonably questioned given the limited sample size. The relationship between SAPCD2 expression level and survival probability were also investigated within the non-MYCN amplified population of patients within the SEQC 498 dataset **(Figure 10)**. The results demonstrate that, like in the overall patient population, a higher expression level of SAPCD2 within the tumor(s) of neuroblastoma patients is associated with poor overall and event-free survival. These results further corroborate the results in the previous Kocak dataset and increase confidence in

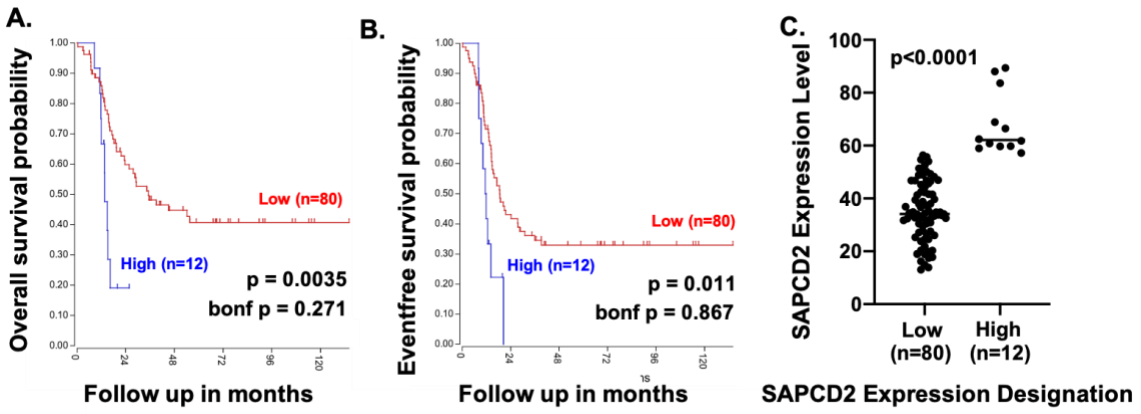

Figure 9. Kaplan-Meier Survival Analysis of MYCN Amplified Neuroblastoma Patients Expressing SAPCD2 in the SEQC Dataset. The population of neuroblastoma patients within the SEQC 498 dataset whose tumors exhibit MYCN amplification at the chromosomal level were separated into two groups based on tumor SAPCD2 mRNA level (high and low) and the resulting survival data was collected over a period of 120 months. **A**, Probability of overall survival in MYCN amplified neuroblastoma patients expressing low (red line) and high (blue line) mRNA levels of SAPCD2. **B**, Probability of event-free survival in MYCN-amplified neuroblastoma patients expressing low (red line) and high (blue line) mRNA levels of SAPCD2. **C**, Expression cutoffs defining each SAPCD2 expression group.

the possibility of SAPCD2 functioning as an oncogene in neuroblastoma.

Finally, the results obtained in the Kocak and SEQC datasets were validated in one additional dataset through the R2 genomics program. The third dataset analyzed was Versteeg 88 (platform u133p2) containing the expression data of 88 neuroblastoma patients in the “tumor neuroblastoma” category. Consistent with the previous two datasets, the correlation between SAPCD2 expression level and survival probability were considered within the overall mixed patient cohort as well as individually in the MYCN amplified and non-MYCN amplified cohorts. **Figure 11** illustrates the Kaplan-Meier survival curves for the

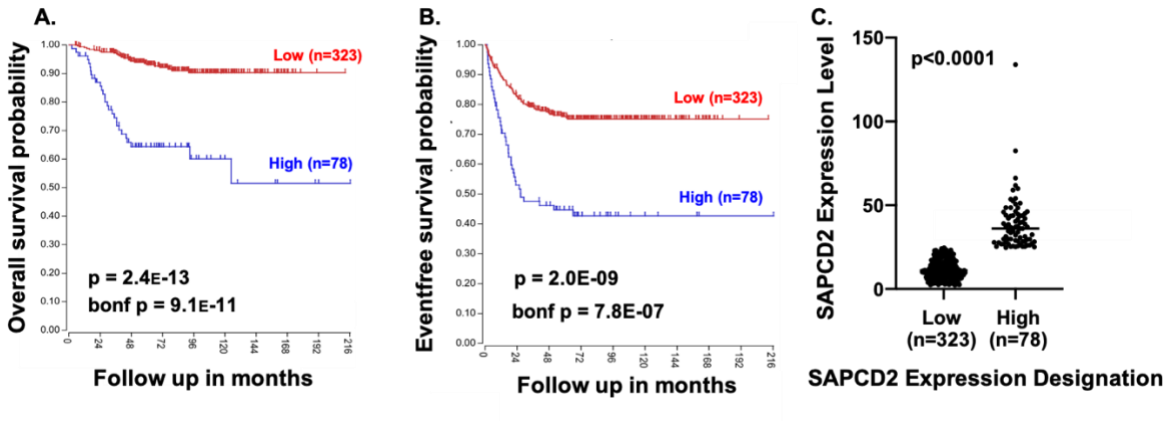

Figure 10. Kaplan-Meier Survival Analysis of non-MYCN Amplified Neuroblastoma Patients Expressing SAPCD2 in the SEQC Dataset. The population of neuroblastoma patients within the SEQC 498 dataset whose tumors do not exhibit MYCN amplification were separated into two groups based on tumor SAPCD2 mRNA level (high and low) and the resulting survival data was collected over a period of 216 months. **A**, Probability of overall survival in non-MYCN amplified neuroblastoma patients expressing low (red line) and high (blue line) mRNA level of SAPCD2. **B**, Probability of event-free survival in non-MYCN amplified neuroblastoma patients expressing low (red line) and high (blue line) mRNA levels of SAPCD2. **C**, Expression cutoffs defining each SAPCD2 expression group.

general patient population within the Versteeg 88 dataset. **Figure 11A-B** indicate that, as with the previous datasets, higher expression levels of SAPCD2 is significantly correlated with a reduction in both overall and event-free survival probability over a period of 216 months. The expression cutoffs illustrated in **Figure 11C** were determined utilizing the same procedure as outlined in previous datasets. The Kaplan-Meier survival data for patients with MYCN amplified tumors is shown in **Figure 12**. Consistent with the Kocak and SEQC datasets, the correlation between high SAPCD2 expression level in neuroblastoma tumors and poor patient survival did not reach statistical significance, likely due to the

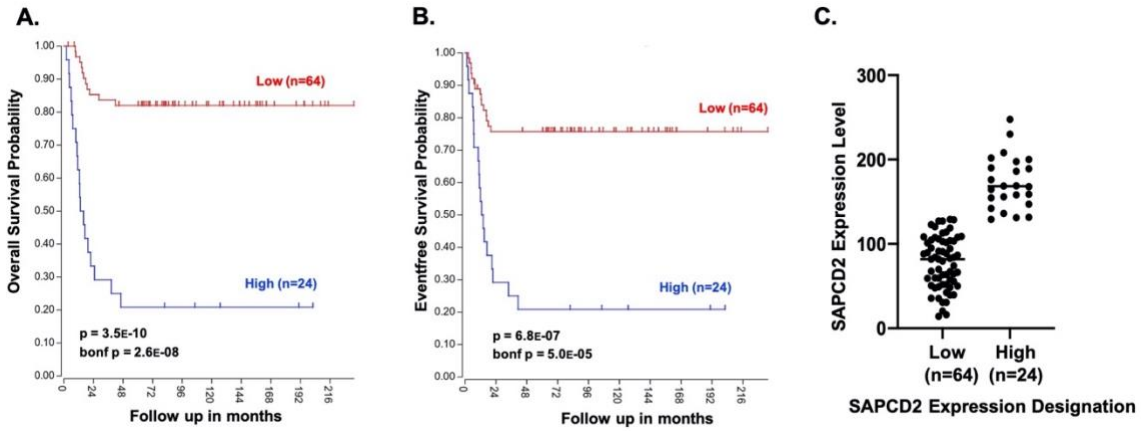

Figure 11. Kaplan-Meier Survival Analysis of Neuroblastoma Patients Expressing SAPCD2 in the Versteeg Dataset. The general population of neuroblastoma patients within the Versteeg 88 dataset were separated into two groups based on tumor SAPCD2 mRNA level (high and low) and the resulting survival data was collected over a period of 216 months. A, Probability of overall survival for neuroblastoma patients expressing low (red line) and high (blue line) mRNA levels of SAPCD2. B, Probability of event-free survival for neuroblastoma patients expressing low (red line) and high (blue line) mRNA levels of SAPCD2. The number of patients in each expression group is indicated in parentheses. C, Expression cutoffs defining each SAPCD2 expression group.

combined effects of reduced statistical power associated with the Bonferroni correction and the naturally small sample size of patients within the MYCN amplified category. Despite this, the relationship between high SAPCD2 expression and lower survival probabilities are qualitatively apparent as in the Kocak and SEQC datasets. The relationship between tumor SAPCD2 expression and poor survival regained statistical significance in the non-MYCN amplified patient category, which includes a much larger sample size **(Figure 13)**. In this category, the relationship between higher SAPCD2 expression and lower survival probabilities are clearly evident, where a higher tumor expression level of

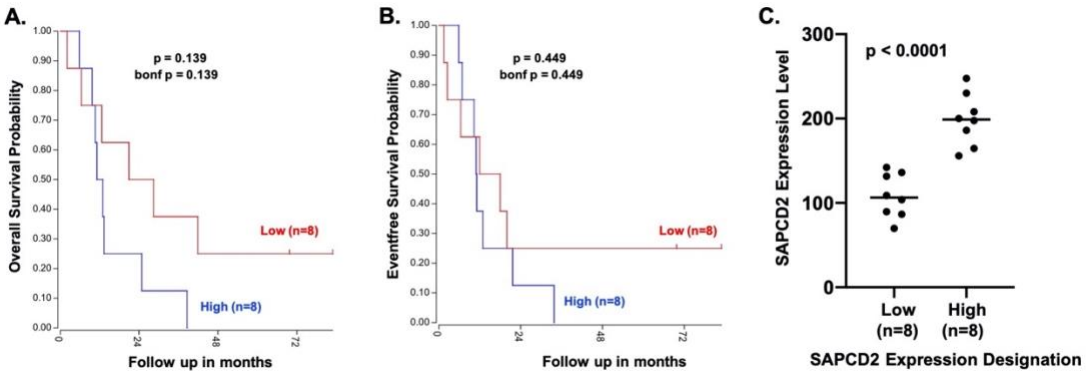

Figure 12. Kaplan-Meier Survival Analysis of MYCN Amplified Neuroblastoma Patients Expressing SAPCD2 in the Versteeg Dataset. The population of neuroblastoma patients within the Versteeg 88 dataset whose tumors exhibit MYCN amplification at the chromosomal level were separated into two groups based on tumor SAPCD2 expression mRNA level (high and low) and the resulting survival data was collected over a period of 72 months. **A**, Probability of overall survival in MYCN amplified neuroblastoma patients expressing low (red line) and high (blue line) mRNA levels of SAPCD2. **B**, Probability of event-free survival in MYCN-amplified neuroblastoma patients expressing low (red line) and high (blue line) mRNA expression levels of SAPCD2. **C**, Expression cutoffs defining each SAPCD2 expression group.

SAPCD2 is associated with a significant reduction in both overall and event-free survival probabilities. These results further corroborate the conclusions made in previous datasets. The consistency in results throughout three independent datasets containing a total of 1,062 neuroblastoma patients provides support for the oncogenic role of SAPCD2 in neuroblastoma and justifies pursuing further investigation through *in vitro* experiments.

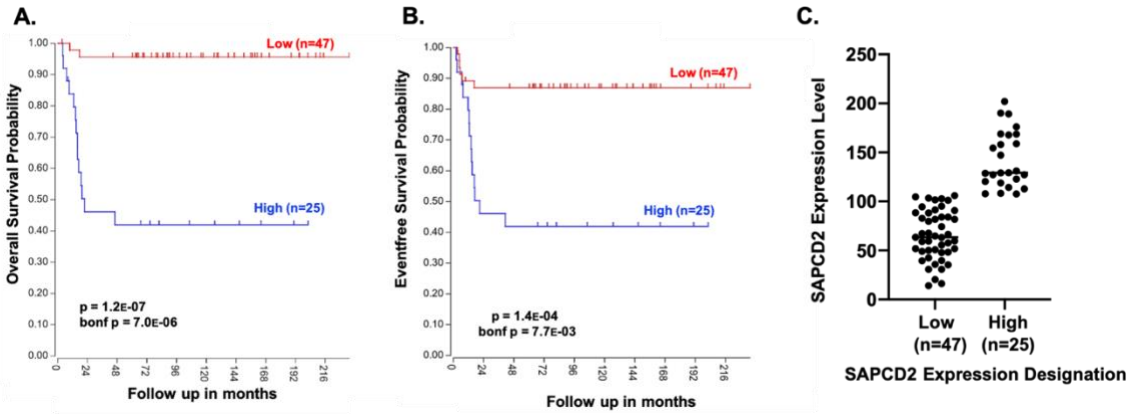

Figure 13. Kaplan-Meier Survival Analysis of non-MYCN Amplified Neuroblastoma Patients Expressing SAPCD2 in the Versteeg Dataset. The population of neuroblastoma patients within the Versteeg 88 dataset whose tumors do not exhibit MYCN amplification were separated into two groups based on tumor SAPCD2 mRNA level (high and low) and the resulting survival data was collected over a period of 216 months. **A**, Probability of overall survival in non-MYCN amplified neuroblastoma patients expressing low (red line) and high (blue line) mRNA levels of SAPCD2. **B**, Probability of event-free survival in non-MYCN amplified neuroblastoma patients expressing low (red line) and high (blue line) mRNA levels of SAPCD2. **C**, Expression cutoffs defining each SAPCD2 expression group.

In vitro SAPCD2 Knockdown Results

The results from our genomic investigations support an oncogenic role for SAPCD2 that contributes to poor prognosis in pediatric neuroblastoma. However, making meaningful conclusions from this data alone is heavily constrained by the limitations of retrospective analysis, particularly when attempting to isolate the effects of a single gene on treatment outcomes against a highly heterogeneous and complex disease. Therefore, while each of the three datasets led to the same conclusions on the effect of SAPCD2 expression on survivability, these results require rigorous *in vitro* validation.

We utilized two human neuroblastoma cell lines in our *in vitro* research. The BE(2)-C cell line is derived from a bone marrow biopsy taken from a 2-year-old male with disseminated neuroblastoma in 1972. It is an adherent cell line and was selected for its ease in culturing and ability to grow neurites when transfected with miR-506-3p, a known inducer of neuronal differentiation in neuroblastoma [105]. All *in vitro* experiments were first conducted in triplicates within the BE(2)-C cell line before validation in the second cell line. The KELLY cell line is derived from the brain and was selected for its ease in culturing. Both cell lines exhibit genomic amplification of MYCN with elevated levels of N-myc protein.

Four commercial siRNAs targeting regions of the SAPCD2 mRNA transcript were selected for use in transfection experiments. Two siRNAs were purchased from Origene and are referred to as Origene siR-1 and Origene siR-3 throughout the study. Two other siRNAs were purchased from Integrated DNA

Technologies and are referred to as IDT siR-131 and IDT siR-132 throughout the study. The full sequences of each siRNA can be found in the materials and methods section, and **Figure 13** illustrates a target map of each of the four siRNAs along the SAPCD2 mRNA transcript. Origene siR-3 and IDT siR-132 target the same region of the mRNA. The negative controls utilized in this study

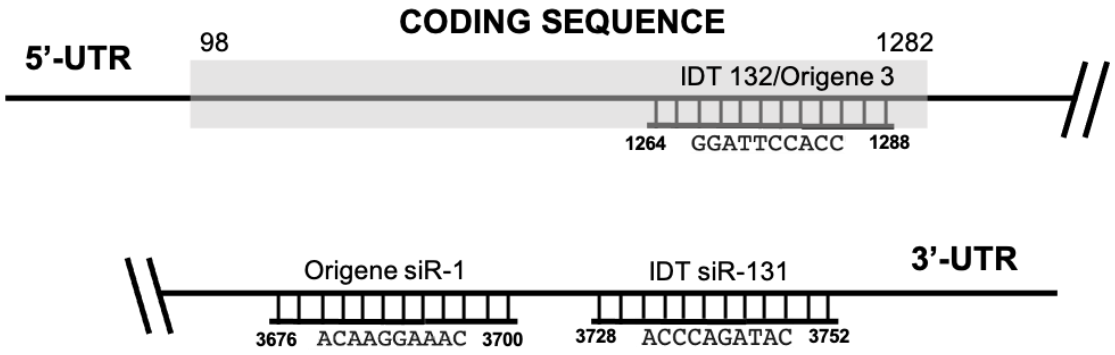

Figure 14. Target Map of siRNAs. Four commercial siRNAs are utilized in this thesis work. The positions along the SAPCD2 mRNA transcript, as well as partial target sequences, are illustrated above. The size of target sequences relative to the mRNA transcript are not drawn to scale.

include “control oligo” and “mock”. The control oligo is a commercial siRNA with a scrambled nucleotide sequence that has been validated to not target any known human gene. The purpose of this negative control is to account for toxicity associated with transfecting any type of regulatory RNA into live cells. The mock (or mock transfectant) control is composed of the lipid nanoparticle transfectant reagent without siRNA and is administered in the same manner in which it is used with siRNAs. The purpose of this negative control is to validate that any changes to cell viability or proliferation cannot be explained by toxicity associated with lipid nanovector transfection reagents.

Performing a transfection with siRNAs targeting SAPCD2 and confirming knockdown at the mRNA and protein levels is a necessary first step in exploring the oncogenic function of SAPCD2 in neuroblastoma. To do this, BE(2)-C cells were separately transfected with the four commercially available siRNAs and allowed to grow for approximately 72 hours at physiological conditions before total RNA and protein isolation. Because isolated RNA is highly unstable and prone to rapid degradation, all isolated RNA samples were subjected to assessment of purity, quality, and structural integrity prior to use in downstream experiments. The concentrations of each individual RNA sample as well as relevant spectrophotometric ratios are reported in **Table 8**. The A260/A280 ratio,

Table 8. Concentration and Purity Assessment of Total RNA Extracted from BE(2)-C Cells

Sample	Concentration	A260/A280	A260/A230
Control Oligo	2,114.5 ng/μL	2.00	1.93
Mock Transfectant	1,932.3 ng/μL	2.00	2.07
Origene siR-1	1,335.5 ng/μL	2.02	2.12
Origene siR-3	982.6 ng/μL	2.03	2.17
IDT siR-131	2,078.1 ng/μL	2.01	2.16
IDT siR-132	1,393.9 ng/μL	2.01	2.22

which measures the ratio of nucleic acids to proteins in a sample, is a standard measure of assessment in predicting the purity of extracted RNA samples for use in downstream applications such as PCR. Total extracted RNA is typically

considered to be of acceptable purity when the A260/A280 ratio is roughly 2.0 [106]. The A260/A230 ratio measures the ratio of nucleic acids to other contaminants that absorb strongly at 230 nm. The A260/A280 and the A260/A230 ratios from the BE(2)-C RNA were considered satisfactory for use in downstream experiments. In addition to RNA purity, structural integrity and overall quality of RNA should be considered prior to utilization in PCR **(Figure 15)**. Each isolated total RNA sample from BE(2)-C was subjected to agarose gel

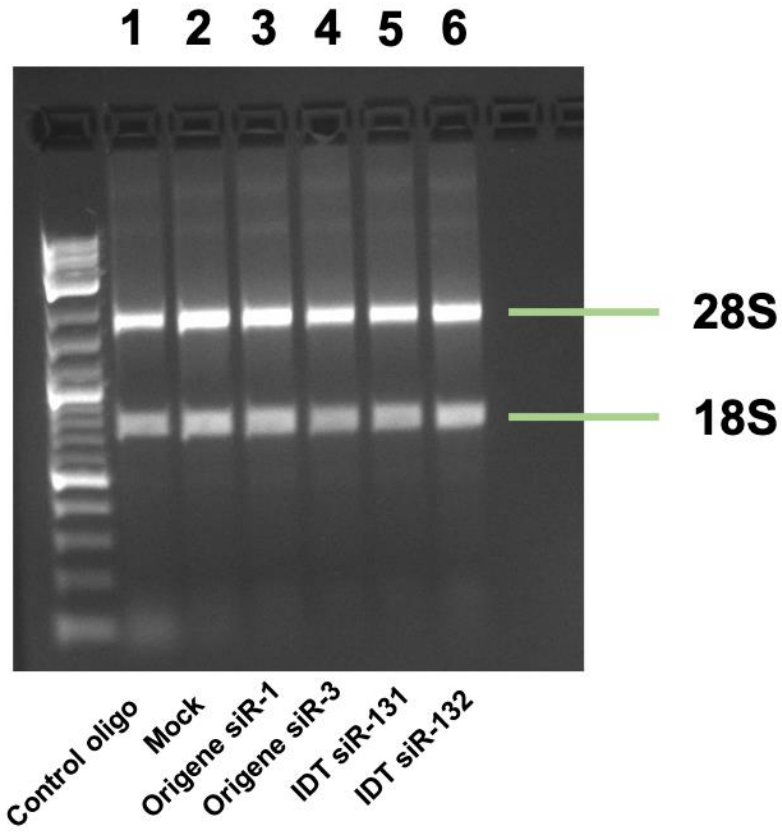

Figure 15. Agarose Gel Electrophoresis to Confirm Quality and Structural Integrity of RNA in BE(2)-C Cells. Following phenol-chloroform RNA isolation using TRIzol, RNA samples were subjected to agarose gel electrophoresis under non-denaturing conditions. Samples were run in fresh 1X TAE buffer at 100 V for 35 minutes.

electrophoresis to validate structural integrity. The integrity of isolated RNA was confirmed by the presence of two distinct bands corresponding to mammalian 28S and 18S ribosomal RNA, where the band corresponding to the 28S ribosome is approximately twice the intensity of the band corresponding to the 18S ribosome **(Figure 15)**. Other small RNAs can be seen as faint smears at the bottom of the gel. Agarose gel electrophoresis of all RNA samples isolated from BE(2)-C under non-denaturing conditions confirms sufficient quality and structural integrity in all samples to proceed with reverse transcription and quantitative PCR. To assess gene expression at the mRNA level, quantitative reverse transcription PCR (qRT-PCR) is preferred over traditional PCR. While traditional PCR involves isolation of DNA from a sample, it is mostly useful for determining whether a specific gene product exists in the sample and whether amplification at the chromosomal level is present. Assessment of SAPCD2 from isolated DNA does not allow for evaluation of expression levels. In qRT-PCR, extracted RNA is reverse transcribed with random primers and reverse transcriptase enzyme to complementary DNA (cDNA), where it is utilized as template DNA in real-time PCR with SYBR green reagents. The amount of cDNA, and thus template DNA, that is utilized in the PCR reaction is directly proportional to the degree of mRNA transcription, which provides a reliable assessment of gene expression at the mRNA level. The reverse transcriptase experiment was performed on each isolated RNA sample and allowed to proceed overnight. The resulting cDNA was utilized in real-time PCR with a commercial SYBR green reagent **(Figure 16)**. Each of the four siRNAs caused a dramatic

reduction in SAPCD2 mRNA levels compared to the control in the BE(2)-C cell line and the results were validated through two independent transfection and qRT-PCR experiments. The results demonstrate that transfection of a human neuroblastoma cell line with each of the four siRNAs successfully reduces SAPCD2 expression at the mRNA level.

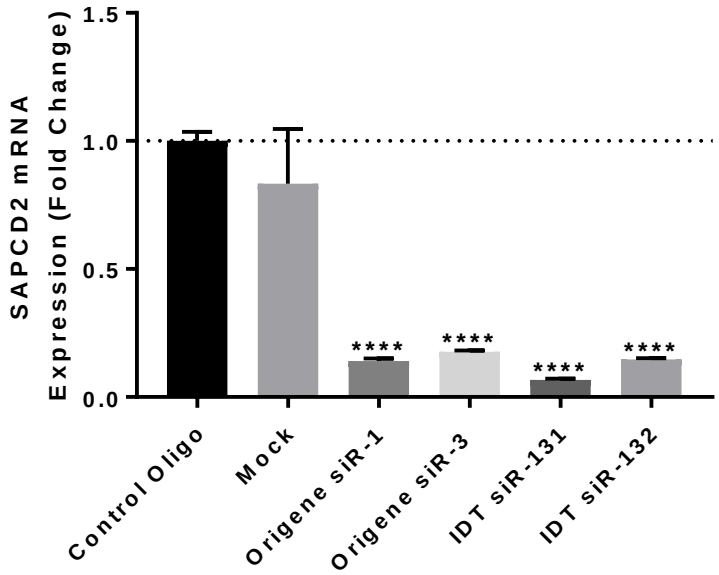

Figure 16. Transfection of BE(2)-C Cells with siRNAs Targeting SAPCD2 Causes a Dramatic Reduction in SAPCD2 Expression at the mRNA Level. Total RNA was extracted from BE(2)-C cell 72 hours following transfection with indicated siRNAs. RNA was assessed for purity and structural integrity before undergoing reverse transcription. The resulting cDNA was utilized in real-time PCR with SYBR green. Results were run in triplicates. ****P <0.0001.

Next, the effect of siRNA-mediated SAPCD2 knockdown on protein levels was evaluated. This experiment was set up in duplicates, where each transfection was carried out in exactly the same manner in two separate 60 mm dishes. One set of 60 mm dishes was utilized for RNA extraction, and the other was utilized for protein extraction. Both extractions took place at roughly the

same time post-transfection in an effort to obtain a reliable assessment of changes to mRNA and protein expression levels following knockdown. In BE(2)-C cells, each of the four tested siRNAs caused a dramatic reduction in the protein levels of SAPCD2 roughly 72 hours post-transfection **(Figure 17)**. These results were validated by multiple separate transfection and western blotting experiments and indicate that each of the four siRNAs are effective in significantly reducing SAPCD2 expression at both the mRNA and protein levels.

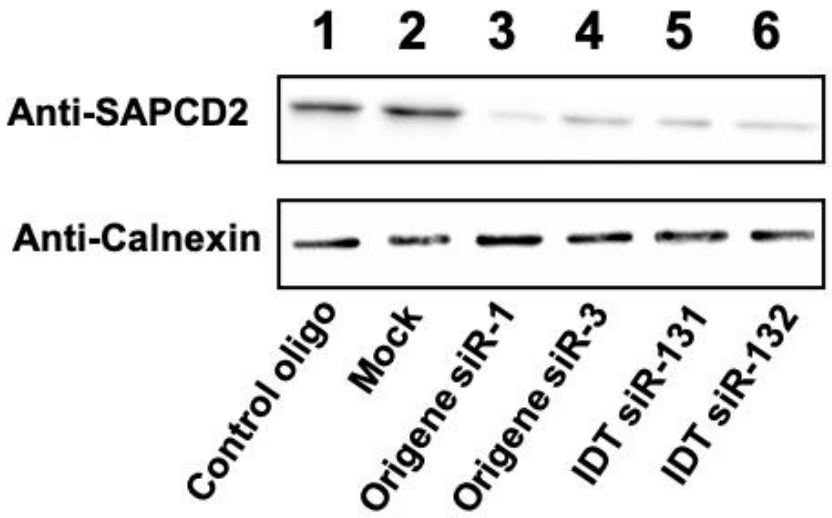

Figure 17. Transfection of BE(2)-C Cells with siRNAs Targeting SAPCD2 Causes a Dramatic Reduction in SAPCD2 Expression at the Protein Level. Protein was collected from BE(2)-C cell lysate 72 hours following transfection with indicated siRNAs and subjected to polyacrylamide gel electrophoresis at 100 V for 80 minutes. Following transfer to PVDF membranes, samples were blotted with anti-SAPCD2 rabbit polyclonal antibodies and visualized with HRP-conjugated anti-rabbit secondary antibodies.

Next, the results were further validated in a second human neuroblastoma cell line. Because each of the four siRNAs reduced SAPCD2 expression at the mRNA and protein levels with approximately equal efficiency, only two of the

siRNAs were selected for testing in the KELLY cell line. First, KELLY cells were transfected according to the forward transfection protocol with IDT siR-131 and IDT siR-132. The cells were allowed to grow for 72 hours before collection of total RNA and protein from cell lysates. The purity, quality, and structural integrity of total RNA extracted from KELLY cells was assessed as described above **(Table 9)**. Similar to the results obtained in the BE(2)-C cell line, the RNA extracted from KELLY cells had optimal A260/A280 ratios of roughly 2.0, indicating acceptable purity for use in qRT-PCR. A lower A260/A230 ratio was

Table 9. Concentration and Purity Assessment of Total RNA Extracted from KELLY Cells

Sample	Concentration	A260/A280	A260/A230
Control Oligo	217.0 ng/μL	2.02	1.44
Mock Transfectant	249.6 ng/μL	2.04	2.27
IDT siR-131	161.0 ng/μL	1.99	1.70
IDT siR-132	88.5 ng/μL	2.02	1.44

noted in three of the samples, however, qRT-PCR is generally considered to be less sensitive to contaminants associated with absorbance in the 230 nm region. Because total RNA was extracted utilizing the phenol-chloroform method, it is likely that the lower A260/A230 ratios are a result of trace phenol remaining in the samples. The structural integrity of the RNA samples was assessed by non-denaturing agarose gel electrophoresis as done previously to confirm that the samples were of sufficient quality to proceed with the qRT-PCR experiment

(Figure 18). Each of the total RNA samples exhibited two distinct bands

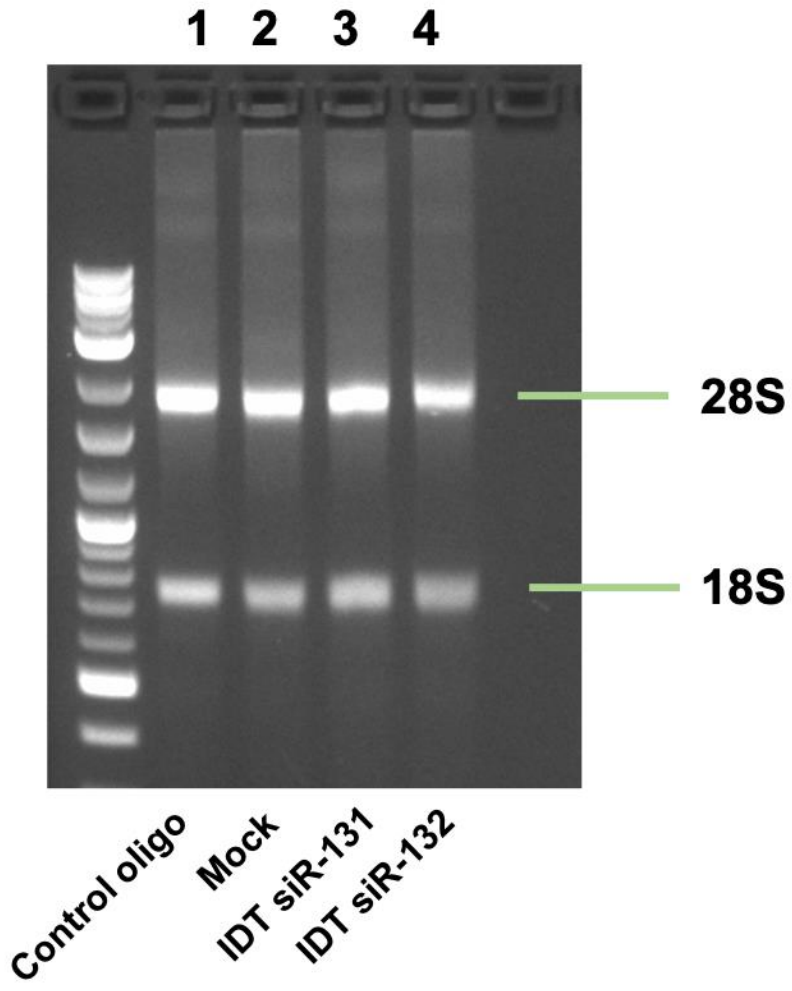

Figure 18. Agarose Gel Electrophoresis to Confirm Quality and Structural Integrity of RNA in KELLY Cells. Following phenol-chloroform RNA isolation using TRIzol, RNA samples were subjected to agarose gel electrophoresis under non-denaturing conditions. Samples were run in fresh 1X TAE buffer at 100 V for 35 minutes.

corresponding to 28S and 18S ribosomal RNA, and the intensity ratio between the 28S and 18S bands were roughly 2 for all samples, consistent with high-quality RNA. In each of the four samples assessed, very faint bands appear in pairs of the same size at a high molecular weight. Because non-denaturing gels

were utilized to assess RNA integrity, these pairs of bands most likely represent RNA secondary structures that are not disrupted prior to electrophoresis. While denaturing RNA gels are generally the accepted standard for assessing quality and structural integrity of extracted RNA, they are difficult and expensive to make and require special handling due to the use of toxic reagents such as formaldehyde [107]. While non-denaturing gels eliminate many of the common obstacles associated with denaturing gels, they do not eliminate RNA secondary structures such as hairpins, pseudoknots, and internal loops. The bands appearing at the top of each lane in **Figure 18** are unlikely to represent genomic DNA contamination for a few reasons. First, on a gel stained with ethidium bromide, genomic DNA typically appears as bright bands rather than faint bands. Secondly, the arrangement of the faint bands in pairs of roughly identical size across all samples is most consistent with the presence of RNA multimers and secondary structures. Because each of the samples were determined to be of reasonable purity (as determined by the A260/A280 ratios) and reasonable structural integrity (as determined by non-denaturing gel electrophoresis), each of the samples were utilized in qRT-PCR to confirm SAPCD2 knockdown at the mRNA level **(Figure 19)**. The results demonstrated that the IDT siRNAs 131 and 132 caused roughly a four-fold decrease in SAPCD2 mRNA levels compared to both negative controls.

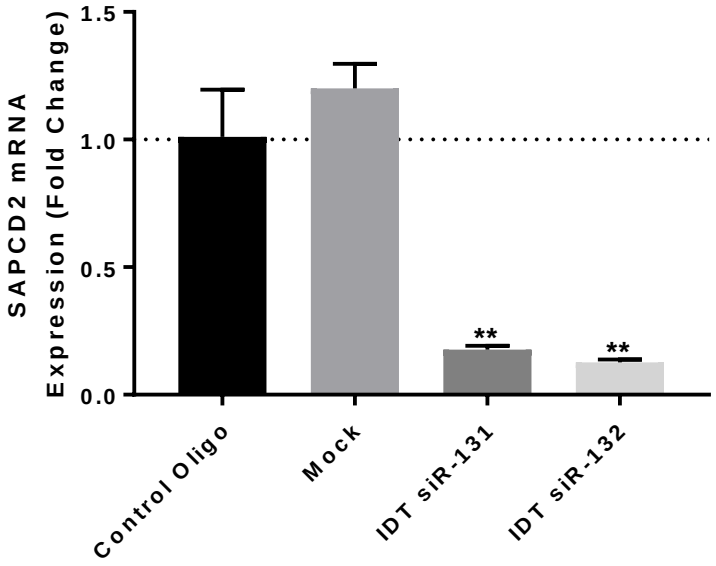

Figure 19. Transfection of BE(2)-C Cells with siRNAs Targeting SAPCD2 Causes a Dramatic Reduction in SAPCD2 Expression at the mRNA Level. Total RNA was extracted from BE(2)-C cell 72 hours following transfection with indicated siRNAs. RNA was assessed for purity and structural integrity before undergoing reverse transcription. The resulting cDNA was utilized in real-time PCR with SYBR green. Samples were run in triplicates. ***P* <0.01.

Next, we analyzed changes in SAPCD2 expression at the protein levels by western blotting **(Figure 20)**. KELLY cells were transfected with IDT siRNAs 131 and 132 and two negative controls in two sets of 60 mm cell culture dishes. Approximately 72 hours after transfection, one set was utilized for RNA extraction and the second set was reserved for protein extraction at roughly the same time point post-transfection. The results demonstrated that SAPCD2 expression is downregulated at the protein level following transfection with siRNAs targeting SAPCD2, but not when transfected with a control oligo with a scrambled target sequence or with the empty lipid nanoparticle transfecting reagent (Mock). These results are consistent with the qRT-PCR results discussed previously in **Figure**

19, and together suggest that siRNA-mediated knockdown of SAPCD2 *in vitro* causes a dramatic reduction in SAPCD2 expression levels at both the mRNA and protein levels within 72 hours. Furthermore, these results corroborate the conclusions made in the previous cell line on the effect of SAPCD2-specific siRNAs on SAPCD2 mRNA and protein expression levels.

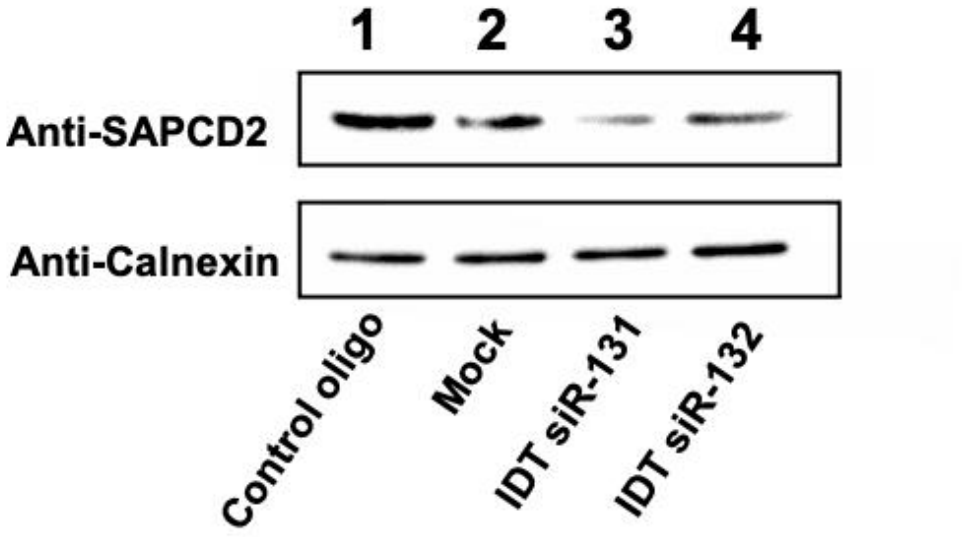

Figure 20. Transfection of KELLY Cells with siRNAs Targeting SAPCD2 Causes a Dramatic Reduction in SAPCD2 Expression at the Protein Level. Protein was collected from KELLY cell lysate 72 hours following transfection with indicated siRNAs and subjected to polyacrylamide gel electrophoresis at 100 V for 80 minutes. Following transfer to PVDF membranes, samples were blotted with anti-SAPCD2 rabbit polyclonal antibodies and visualized with HRP-conjugated anti-rabbit secondary antibodies.

SAPCD2 Effect on Neuroblastoma Cell Survival, Differentiation, and Proliferation Results

Following confirmation of successful reduction in SACPD2 expression at the mRNA and protein levels after siRNA transfection *in vitro*, the next step was to determine the phenotypic consequences that result from SAPCD2 depletion.

Given previous literature identifying SAPCD2 as a driver of a variety of oncogenic events in several cancers, we hypothesized that SAPCD2 contributes to neuroblastoma cell survival and proliferation at the cellular level. Additionally, we sought to determine whether SAPCD2 has a significant effect on the differentiation status of neuronal precursors. Because the differentiation status of neuronal precursors is a major factor in staging neuroblastoma tumors, recent attention has been given towards identifying proteins and cell signaling pathways that modulate the neuronal differentiation process.

Utilizing the same human neuroblastoma cell lines BE(2)-C and KELLY, we performed colorimetric cell viability experiments to determine the effect of SAPCD2 knockdown on neuroblastoma cell survival and clonogenic (colony formation) assays to measure the effect of SAPCD2 knockdown on proliferative capacity. Morphological changes following siRNA-mediated knockdown were assessed to predict any changes in differentiation status upon depletion of SAPCD2.

All experiments were first carried out in the BE(2)-C cell line utilizing all four siRNAs with at least two independent replicates. Following this, each experiment was repeated in the KELLY cell line utilizing the same two IDT siRNAs analyzed in the previous section.

The siRNA-mediated knockdown of SAPCD2 on neuroblastoma cell viability was assessed by MTT assay **(Figure 21)**. Compared to the two negative controls, each of the four siRNAs caused a dramatic reduction in cell survival following SAPCD2 depletion. These results were replicated in multiple separate

transfection experiments. MicroRNA 506-3p (miR-506-3p) is an appropriate positive control for use in viability, proliferation, and differentiation experiments as it is known to function as a potent differentiation inducing agent in neuroblastoma [105]. Additionally, it successfully reduces cell survival and was utilized as a positive control in all MTT metabolic assays.

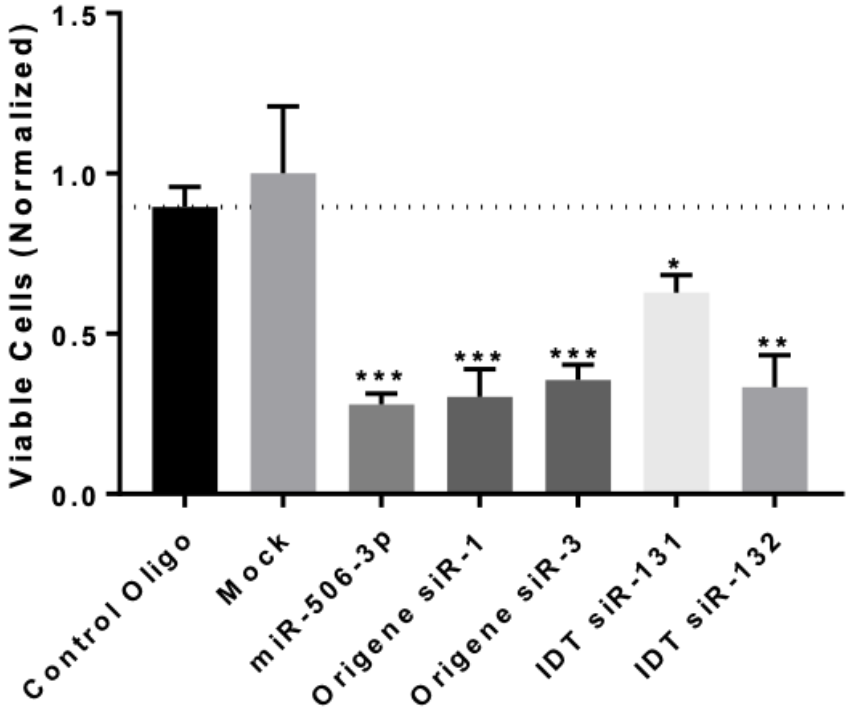

Figure 21. Knockdown of SAPCD2 Reduces Neuroblastoma Cell Viability in the BE(2)-C Cell Line. 4,000 neuroblastoma cells from the BE(2)-C cell line were transfected with indicated siRNAs in a 96-well plate and grown at physiological conditions for four days. Relative viability was measured by MTT colorimetric assay and spectrophotometric analysis at 570 nm with a reference wavelength of 630 nm. *P <0.05, **P <0.01, ***P < 0.001.

In addition to changes in cell survival following SAPCD2 depletion, the effect of SAPCD2 in modulating neuronal differentiation was measured qualitatively by assessing morphological changes to neuroblastoma cells

following SAPCD2 knockdown *in vitro*. As neural crest-derived precursors of the nervous system, neuroblastoma cells may display morphological characteristics along a continuum of traits associated with various stages of the differentiation process. Poorly differentiated neuroblastoma cells are characterized by irregular cell boundaries, extensive clustering, and little to no neurite growth. Well-differentiated cells, on the other hand, display significantly reduced cell body surface area, little to no clustering, and profound neurite projections. These morphological changes may be assessed qualitatively by imaging with an Incucyte® ZOOM Live Cell Analysis System **(Figure 22)**. Following reverse transfection of neuroblastoma cells in a 96-well plate, 9 images were obtained for each well. A pre-set processing definition specific to analyzing neurite outgrowth in BE(2)-C neuroblastoma cells was previously created by our lab and utilized for assessment in this cell line. When the processing definition is applied to the images obtained by the Incucyte instrument, the software automatically detects cell bodies and applies a yellow mask to distinguish them from the greyscale background. Similarly, neurite projections are detected automatically and colored in magenta. The results presented in **Figure 22** indicate that the miR-506-3p positive control caused a dramatic advancement in neuroblastoma cell differentiation as measured by neurite outgrowth and significant reductions in cell body volumes, confirming that the transfection was successful and the morphological changes associated with an advancement of differentiation were clearly evident in the positive control. However, none of the four siRNAs tested resulted in significant changes in differentiation status. This experiment was

repeated multiple times with consistent results, in which each of the four siRNAs successfully reduced cell survival without causing significant neurite outgrowth to indicate an advancement in differentiation. This result indicates that SAPCD2 contributes to neuroblastoma cell survival but is not likely a direct regulator of neuronal differentiation.

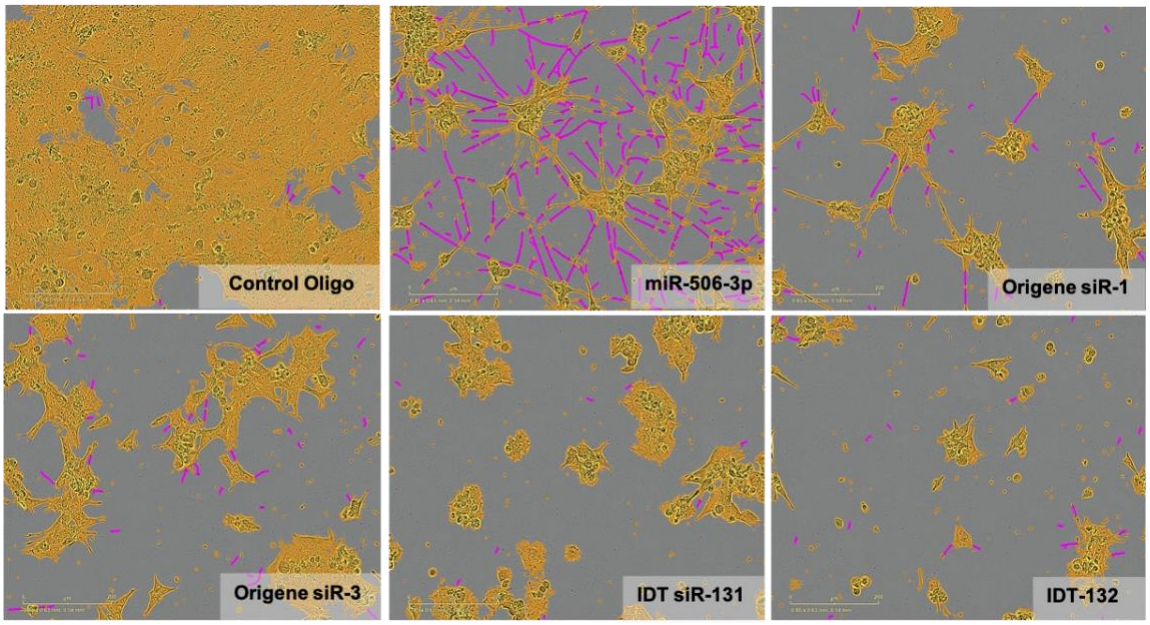

Figure 22. Changes to Neuroblastoma Cell Morphology Following SAPCD2 Depletion in BE(2)-C Cells. 4,000 neuroblastoma cells from the BE(2)-C cell line were transfected with indicated siRNAs in a 96-well plate and grown at physiological conditions for four days. Cell morphology was measured by imaging with an Incucyte® ZOOM Live Cell Analysis System.

Next, the effect of SAPCD2 on regulating neuroblastoma cell proliferation was measured with a colony formation or clonogenic assay **(Figure 23)**. In this assay, neuroblastoma cells are seeded at very low densities and allowed to grow at physiological conditions for two weeks. Cells possessing a high proliferative index form extensive colonies, which are stained with a crystal violet solution. The results demonstrated in **Figure 23** indicate that knockdown of SAPCD2 *in*

vitro reduces the proliferative capacity of neuroblastoma cells in the BE(2)-C cell line as measured by a significant reduction in both neuroblastoma colony size and number. These results were later replicated in a separate colony formation assay utilizing two additional siRNAs against SAPCD2 **(Figure 24)**. Overall, these results can be further interpreted to demonstrate that SAPCD2 contributes to neuroblastoma cell proliferation in the BE(2)-C cell line.

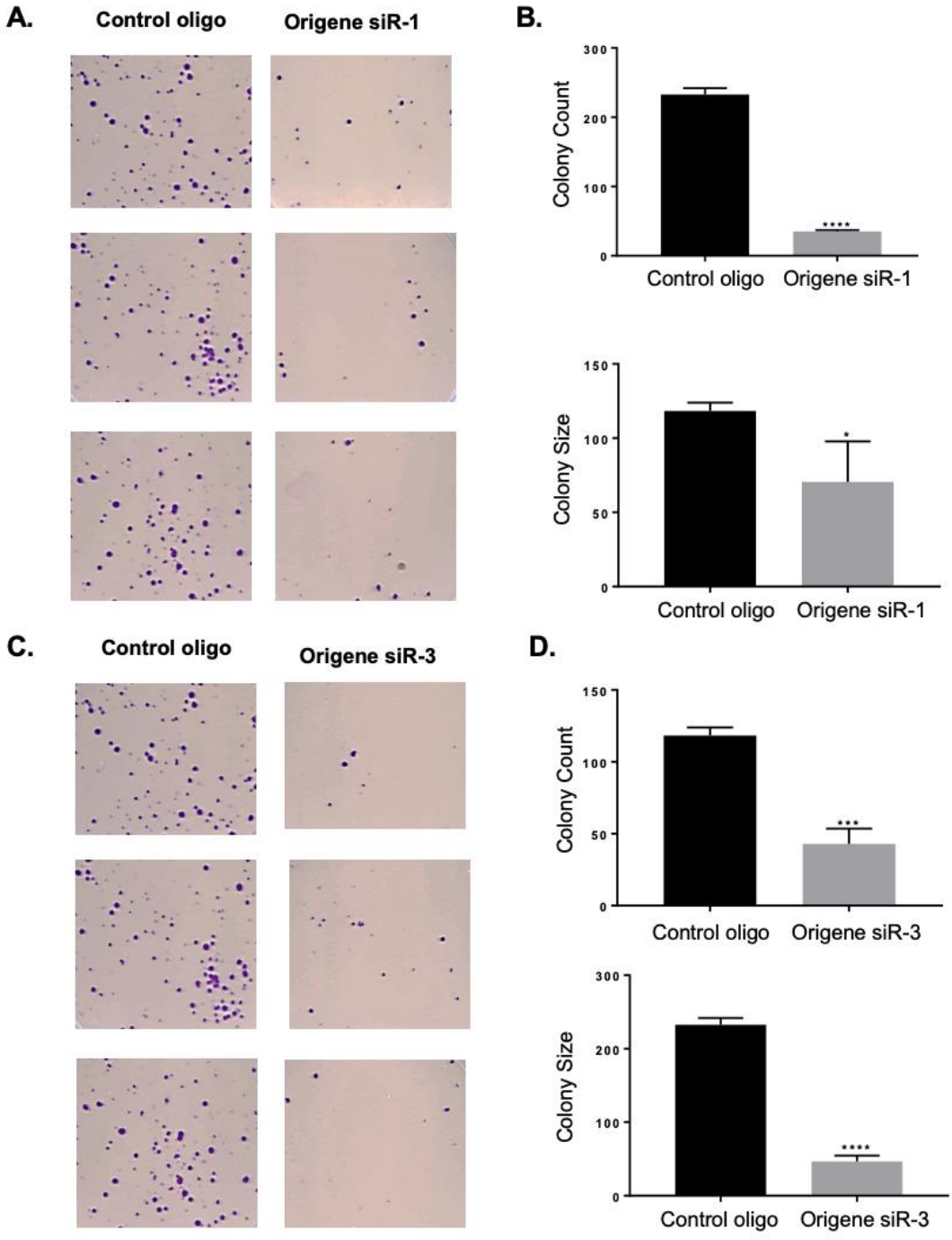

Figure 23. SAPCD2 Knockdown with Origene siRNAs Reduces Neuroblastoma Cell Proliferation in BE(2)-C Cells. 5,000 BE(2)-C cells were transfected with Origene siRNAs 1 and 3 according to the fast forward transfection protocol and seeded at very low densities in 10 cm cell culture dishes. The cells were permitted to grow at physiological conditions for two weeks or until extensive colony growth was evident. Colonies were stained with crystal violet and imaged with a photo scanner. Colony size and number were assessed quantitatively in the ImageJ software. *P <0.05, ***P < 0.001, ****P <0.0001.

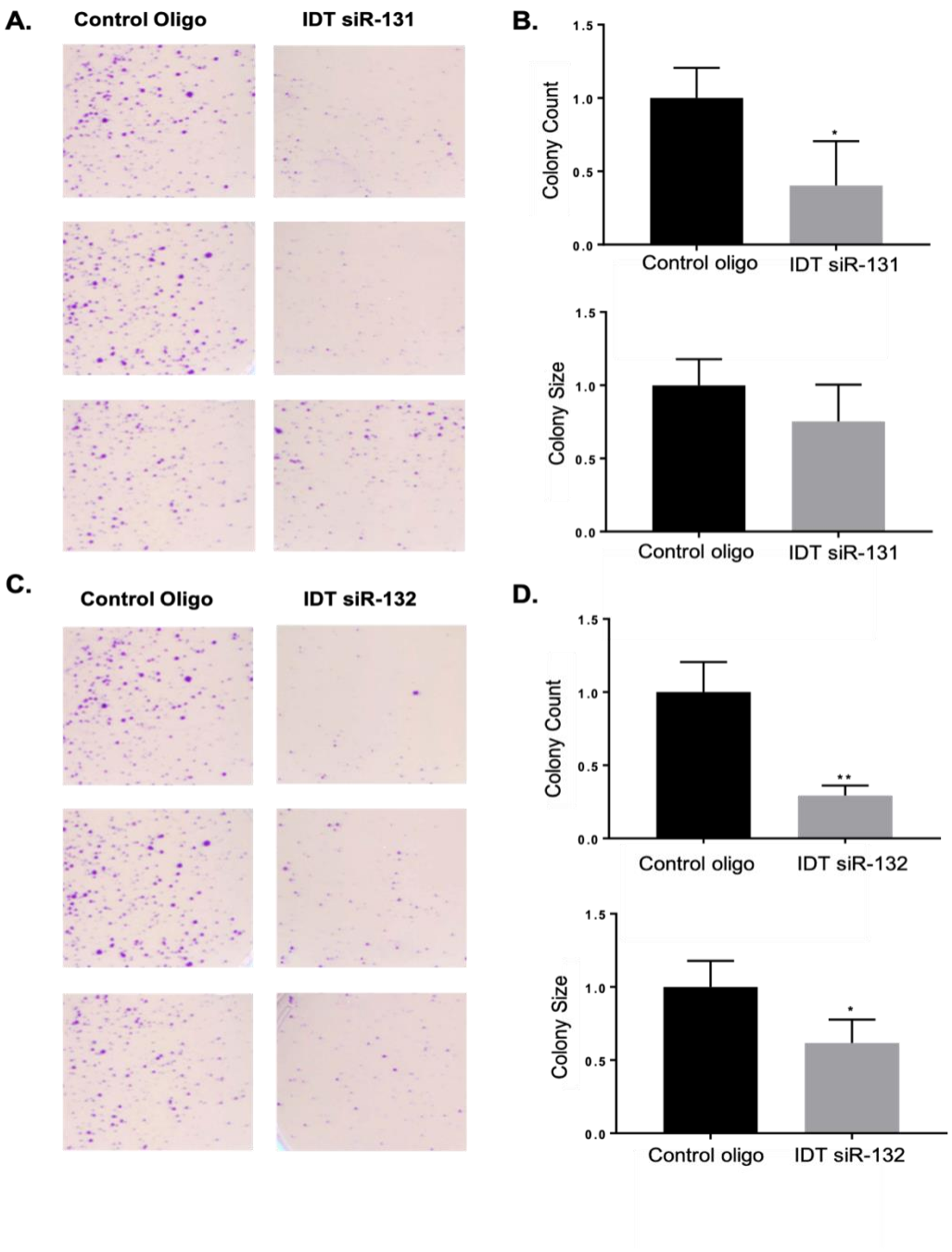

Figure 24. SAPCD2 Knockdown with IDT siRNAs Reduces Neuroblastoma Cell Proliferation in BE(2)-C Cells. 5,000 BE(2)-C cells were transfected with Origene siRNAs 1 and 3 according to the fast forward transfection protocol and seeded at very low densities in 10 cm cell culture dishes. The cells were permitted to grow at physiological conditions for two weeks or until extensive colony growth was evident. Colonies were stained with crystal violet and imaged with a photo scanner. Colony size and number were assessed quantitatively in the ImageJ software. *P <0.05, ***P < 0.001, ****P <0.0001.

In order to further validate our results from cell survival, differentiation, and proliferation assays in the BE(2)-C cell line, we investigated the effect of SAPCD2 knockdown on neuroblastoma cell survival, differentiation, and proliferation in the KELLY cell line using the same experiments described previously. Depletion of SAPCD2 *in vitro* leads to a dramatic reduction of cell viability in the KELLY cell line **(Figure 25)**. Compared to the two negative controls, siRNA-mediated knockdown of SAPCD2 led to a significant reduction in cell viability. Although the phenotypic consequence of SAPCD2 knockdown does not appear as pronounced in the KELLY cell line as in the BE(2)-C cell line, the effect reached statistical significance and was validated by multiple transfection experiments. Notably, the reduction in cell survival as a result of SAPCD2 knockdown by both siRNAs was more prominent than the reduction in cell survival by the positive control.

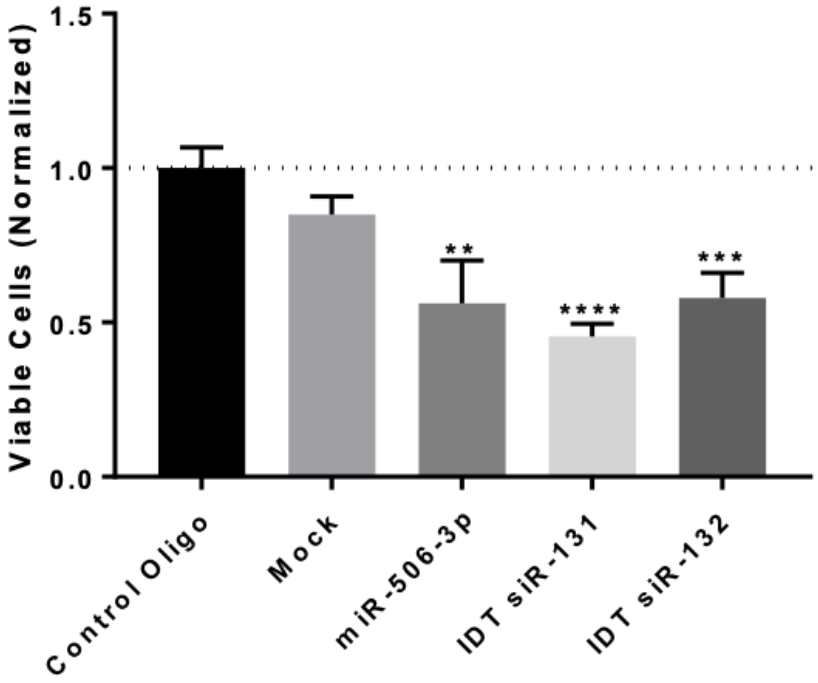

Figure 25. Knockdown of SAPCD2 Reduces Neuroblastoma Cell Viability in the KELLY Cell Line. 4,000 neuroblastoma cells from the KELLY cell line were transfected with indicated siRNAs in a 96-well plate and grown at physiological conditions for four days. Relative viability was measured by MTT colorimetric assay and spectrophotometric analysis at 570 nm with a reference wavelength of 630 nm. ***P* <0.01, ****P* <0.001, *****P* <0.0001.

Next, cell morphology was assessed to determine whether SAPCD2 may play a role in regulating neuroblastoma cell differentiation in the KELLY cell line **(Figure 26)**. The results demonstrate that knockdown of SAPCD2 with both IDT siRNAs caused a noticeable reduction in the number of cells and size of cell clusters, but without significant neurite outgrowth to indicate an advancement in differentiation status. These results corroborate the findings in the BE(2)-C cell line and further suggest that SAPCD2 likely does not play a significant, or at least a direct, role in modulating neuronal differentiation. Like in the BE(2)-C cell line

tested previously, miR-506-3p was utilized as a positive control for assessing morphological changes consistent with advancement in differentiation status. However, the neurite outgrowth upon treatment with the miR-506-3p positive control was not as extensive in the KELLY cell line as in the BE(2)-C cell line, raising the question of whether the more modest effect on cell viability seen in **Figure 25** could be explained by poor transfection efficiency or unfavorable conditions in cell physiology. However, neurite outgrowth in KELLY cells following transfection with miR-506-3p was underrepresented by the Incucyte algorithm. Unlike for the BE(2)-C cell line, a processing definition for measuring

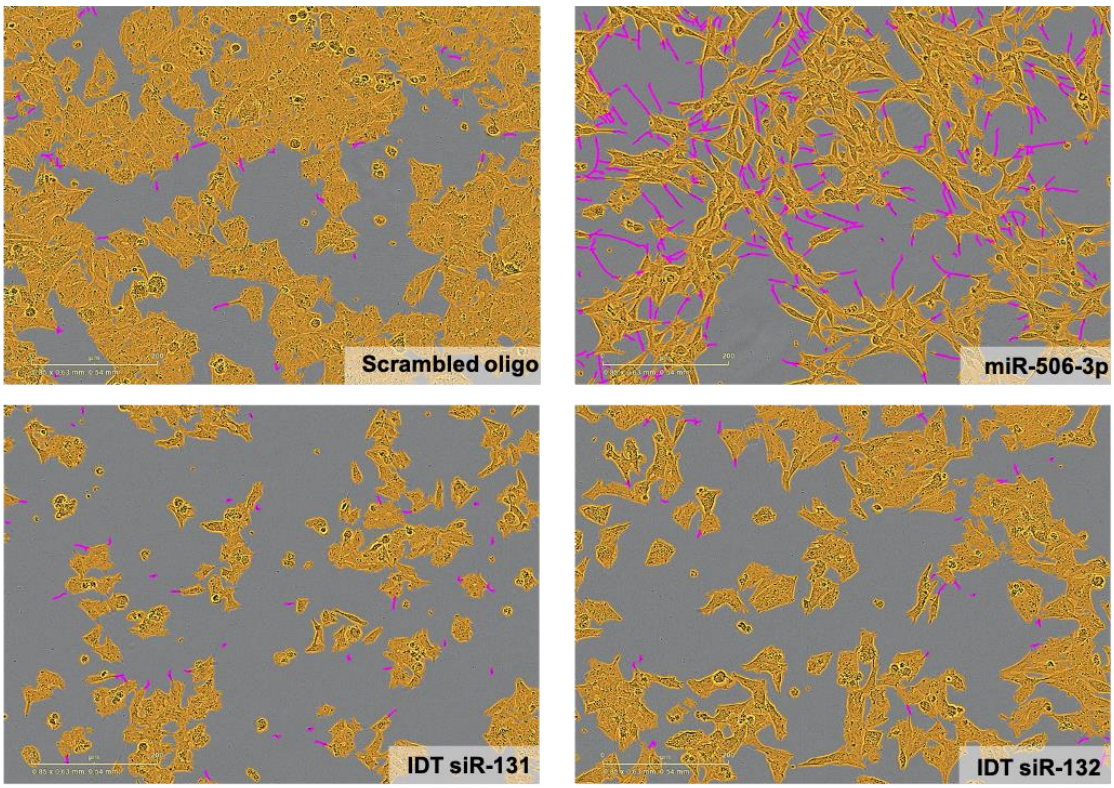

Figure 26. Changes to Neuroblastoma Cell Morphology Following SAPCD2 Depletion in KELLY Cells. 4,000 neuroblastoma cells from the KELLY cell line were transfected with indicated siRNAs in a 96-well plate and grown at physiological conditions for four days. Cell morphology was measured by imaging with an Incucyte® ZOOM Live Cell Analysis System.

neurite outgrowth in the KELLY cell line was not previously established by our lab. The processing definition was manually created and optimized within the IncucyteZoom software with sufficient sensitivity to differentiate between neurites and cell bodies, while reducing excessive sensitivity and preventing background noise. Prior to applying cell body and neurite masks, the greyscale images indicated that neurite outgrowth in response to transfection with miR-506-3p was extensive but differentiated KELLY cells displayed a higher degree of overlap between neurite projections and adjacent cell bodies as well as more complex and extensive webs of neurite growth compared to BE(2)-C cells **(Figure 27)**.

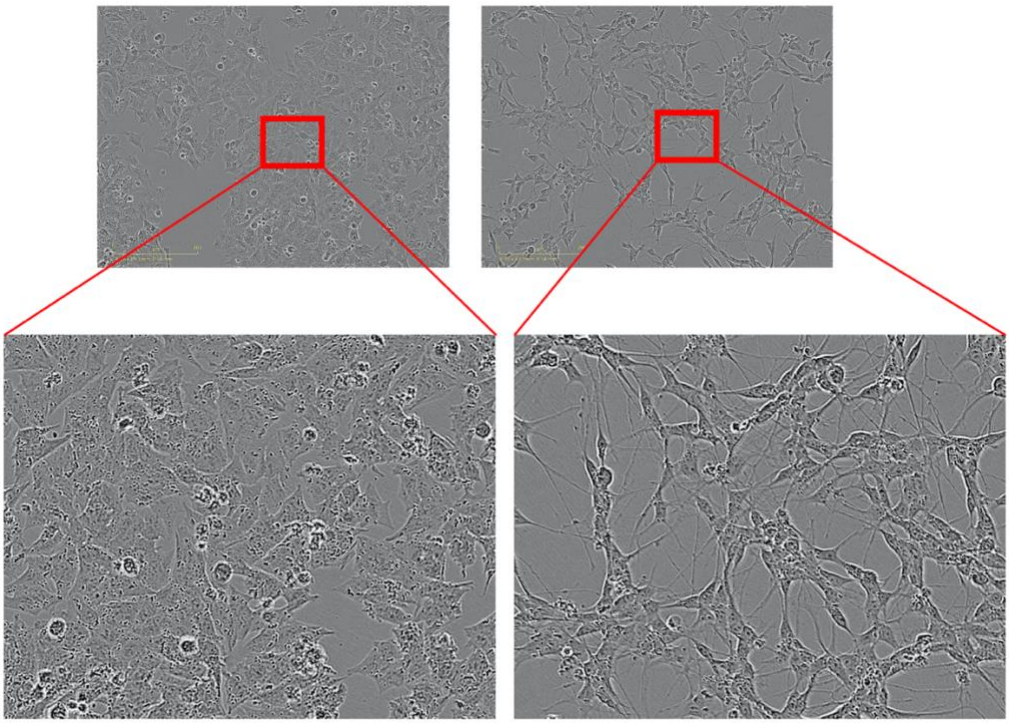

Figure 27. Morphology of the KELLY Cell Line Complicates Data Analysis. Greyscale images of KELLY cells prior to the addition of cell body and neurite masks reveal a complex web of neurite projections with extensive overlap and clustering. **Left**, cells treated with control oligo displaying poor differentiation status. **Right**, cells treated with miR-506-3p positive control displaying advanced differentiation status and complex neurite outgrowth patterns.

Together, these characteristics made it difficult for the Incucyte software to resolve the differences between cell bodies and neurites when layered on top of one another even after thorough optimization. Consequentially, the algorithm overestimated cell body volume and vastly underestimated both the number and length of neurite projections in **Figure 26**, and it can be concluded that the more modest effect of SAPCD2 knockdown on cell viability in the KELLY cell line is not due to poor transfection efficiency or problems with the physiological state of the cells at the time of transfection. Due to the consistency in results obtained in pursuit of determining the effect of SAPCD2 on neuroblastoma cell differentiation, this effect was not further investigated by western blot analysis or other measurements of differentiation status.

IV. DISCUSSION

Neuroblastoma is the most common extra-cranial solid tumor in infants and children and is responsible for 15% of all cancer deaths in the pediatric population. It is characterized by a high degree of cellular heterogeneity and adherence to the clonal evolution model, in which malignant cells undergo genetic and epigenetic diversification that confers a selective advantage in evading growth suppression and acquiring treatment resistance [108, 109]. Because of this, developing therapies against neuroblastoma that are effective for a large number of patients presents a clinical challenge due to the unique genetic profiles of each individual patient and the extensive diversification of tumor biochemistry. Currently approved treatments against neuroblastoma include traditional chemotherapy and radiation as well as immunotherapy. Targeting neuroblastoma through the inhibition of tumor-specific oncogenes such as MYCN has proven to be a successful strategy, but its use is restricted by the diverse genetic profiles of each tumor. The identification of novel oncogenes that are involved in the initiation and progression of neuroblastoma, as well as gaining a more sophisticated understanding of the cell signaling pathways relevant to neuroblastoma, are important steps in the development of new anti-cancer therapies that may be effective for different groups of patients who are excluded from certain therapies due to their individual tumor genetics.

SAPCD2 was first isolated in 2007 and identified as a gene with cell cycle-dependent expression patterns in a human gastric cancer cell line. Since its initial discovery, several other groups have identified it as a differentially expressed

gene in several different types of human cancer cell lines but not in matched normal epithelial or mucosal cells. Furthermore, several other *in vitro* studies have identified SAPCD2 as contributing to the oncogenic and malignant behavior of several types of human cancers and *in vivo* tumor models have further revealed a proliferative function of SAPCD2. While healthy cells have been documented to express SAPCD2 at high levels throughout the early stages of embryonic development, its expression is generally eliminated in normal tissues at the time of birth. Given that neuroblastoma arises from abnormalities in neuronal precursors derived from the process of neurulation around gestational week four, consideration of potential oncogenes specific to embryogenesis in the initiation and progression of neuroblastoma is warranted. Because SAPCD2 has been identified as an oncogene in a variety of human cancers and its expression levels in normal cells are generally confined to the early weeks of fetal development, we hypothesized that SAPCD2 may also function as an oncogene in neuroblastoma.

SAPCD2 is correlated with poor prognosis of neuroblastoma patients

Results from the genomic analysis of more than 1,000 neuroblastoma patients expressing SAPCD2 reveal that higher expression levels are significantly correlated with a reduction in both overall and event-free survival probability. Three independent patient datasets confirmed these results, and high SAPCD2 expression combined with MYCN amplification led to the premature death of all analyzed patients. Because MYCN is a transcription factor involved in

the regulation and activation of important genes involved in the development of tissues and organs, there exists a possibility that SAPCD2 is one gene that is regulated by MYCN. In order to predict whether MYCN is a transcriptional regulator of SAPCD2, DNA sequence analysis was utilized to identify enhancer elements called E-boxes with the consensus sequence CANNTG. These sequences are binding sites for transcription factors adopting basic helix-loop-helix structures, such as MYCN. E-boxes play an especially large regulatory role during neurogenesis and MYCN is known to heterodimerize with MAX at these consensus sequences in neuroblastoma [110, 111]. Putative MYCN target sites within the SAPCD2 promoter region were predicted and are shown in **Table 10**.

Table 10. E-Box Consensus Sequences in the SAPCD2 Promoter. E-boxes with the consensus sequence CANNTG were predicted within the promoter region of SAPCD2 by the ContraV3 web server. Highlighted regions represent E-box consensus sequences. All binding sites are putative and have not been validated by biological experiments.

Target Sequence	Genomic Position	Conservation	Position in Promoter
TGGCCGAGCCCGTC-CCATCTGCTCTCTGATAG	Chr9:139965073-139965124	8 species	~65 bp upstream of start codon
GCGCTTTCTCGGATCCAGCTGTGGCTGGCTGCC	Chr9:139965236-139965317	8 species	~500 bp upstream of start codon
CAGGT-GACCCTGCGGCCCCCTTCTCTTCCACCA	Chr9:139965396-139965458	6 species	~765 bp upstream of start codon
GGATCGTAGGCTCCAGCCAGCTGGGCG	Chr9:139965496-139965548	18 species	~825 bp upstream of start codon

Conservation of E-box sequences across several species increases the likelihood that these elements are truly involved in the regulation of SAPCD2 gene expression. **Figure 28** illustrates each of these E-box sequences within the SAPCD2 promoter region and their relative positions. While time did not allow for further exploration of the regulatory relationship between SAPCD2 and MYCN, it remains an interesting directive for future investigation. Clinically, amplification of the MYCN gene at the chromosomal level as well as elevated expression levels of SAPCD2 may have a synergistic effect in reducing survival probability and worsening prognosis of neuroblastoma patients. If SAPCD2 is a downstream effector of the MYCN transcription factor, this relationship could explain why so few patients exhibiting both MYCN amplification and SAPCD2 overexpression are able to survive beyond the age of 2.

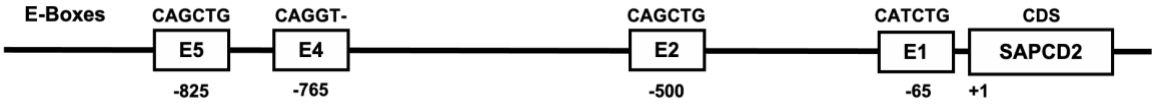

Figure 28. Potential MYCN Target Sites Within the SAPCD2 Promoter. The free online ContraV3 program was utilized to identify E-box elements with the consensus sequence CANNTG within the promoter region of SAPCD2. The transcription start site of the SAPCD2 gene is labeled +1. Consensus sequences are denoted above each E-box and positions within the SAPCD2 promoter are listed below. All E-boxes shown are putative and have not been validated by biological experiments.

While the results of our genomic analysis strongly suggests that SAPCD2 functions as an oncogene in neuroblastoma, it is important to recognize the limitations of retrospective clinical investigations in establishing causal relationships. Not only is it impossible to completely isolate and manipulate dependent and independent variables within patient genomic datasets, but this

type of analysis also severely oversimplifies the complexity of cancer and the multifaceted orchestration of events on the cellular level. Isolating the effects of one single gene on the treatment outcomes of a cancer patient ignores the extensive interactions between cell signaling and gene regulatory networks that come together to impact prognoses. For this reason, it is critically important to further explore the conclusions formed from genomic analysis in biological experiments.

In vitro knockdown of SAPCD2 reduces expression at the mRNA and protein levels

Following the results obtained from genomic analysis, our first goal was to determine whether transfection of a human neuroblastoma cell line with siRNAs successfully reduces SAPCD2 expression at both the mRNA and protein levels. We began testing a selection of commercially-available siRNAs that target the 3'-UTR of SAPCD2 in the human neuroblastoma cell line BE(2)-C. Total RNA to be used in quantitative reverse transcription PCR experiments was extracted from cells in parallel with protein lysate to be used in western blotting to analyze the effect of siRNA on SAPCD2 mRNA and protein expression levels at approximately equal time points. When assessing changes to expression at the mRNA level, it is important to utilize reverse transcription PCR (RT-PCR) rather than traditional PCR. While traditional PCR is a useful tool for detecting the presence of a gene within the genomic DNA, it does not provide useful information on the expression level of a gene, which is regulated at the post-

transcriptional and post-translational levels. Epigenetic modifications can be assessed through chromatin immunoprecipitation (ChIP) assays, but histone methylation patterns are not altered by the introduction of regulatory RNAs. RT-PCR relies upon the transcription of a gene to its mature mRNA transcript, which is then reverse transcribed with random primers to the corresponding cDNA sequence. This way, significant reductions in gene transcription result in small amounts of mature mRNA and, consequently, smaller amounts of template cDNA. For this reason, RT-PCR provides a reliable assessment of mRNA expression levels [112].

Following extraction of total RNA from live cells, it is important to assess the purity and quality of RNA samples prior to use in downstream applications. Traditionally, denaturing agarose gels containing formaldehyde are utilized to disrupt secondary RNA structures that form via intramolecular base pairing, which can alter migration patterns. However, the use of denaturing formaldehyde gels is expensive, time consuming, and involves the use of toxic reagents. For this reason, non-denaturing agarose gels stained with ethidium bromide were utilized to assess RNA quality with the acknowledgement that secondary structures may alter band appearance. We found that the use of non-denaturing agarose gels did not significantly obscure the assessment of sample quality.

While the effects of gene knockdown can be assessed as early as a few hours following transfection with high quality reagents, the generally accepted time interval for assessing knockdown is between 24 and 96 hours [113]. Through our experiments, we determined that 72 hours post-transfection is the

optimal interval for assessing gene knockdown. Each of the four siRNAs successfully reduced SAPCD2 expression levels with an average 5-fold reduction in SAPCD2 mRNA levels as revealed by qRT-PCR. Additionally, multiple western blot experiments indicated reduced protein levels of SAPCD2. Because SAPCD2 is still a relatively novel gene with few published investigations, only three primary antibodies against SAPCD2 are commercially available. Of the three antibodies, one produced optimal signal to noise ratios but exhibited non-specific binding interactions. The western blotting protocol was optimized over a period of several months to determine the best strategies for blocking and primary antibody incubations to maximize signal while minimizing the appearance non-specific bands. We found that prolonged blocking at 4℃ with 5% dry milk in TBST for 48 hours with extended washing steps before and after secondary antibody application achieved optimal results. Additionally, the BE(2)-C cell line exhibited more non-specific protein binding than the KELLY cell line, which reflects the unique genetic profiles of each neuroblastoma patient.

SAPCD2 Depletion reduces neuroblastoma cell viability and proliferation

After determining that each siRNA successfully reduced SAPCD2 expression at the mRNA and protein levels, we next sought to determine how SAPCD2 depletion impacted the viability and proliferative capacity of neuroblastoma cells. Following confirmation that each of the four siRNAs successfully reduces SAPCD2 expression level within the BE(2)-C cell line, two of the four siRNAs were selected for testing in the KELLY cell line. We found that siRNA-mediated knockdown of SAPCD2 significantly reduced neuroblastoma cell

survival in the BE(2)-C cell line with an average 2-fold reduction in relative viability. These results were replicated in several independent experiments within the BE(2)-C cell line, providing strong indication that SAPCD2 contributes to cell survival in neuroblastoma. However, the KELLY cell line appeared to display a far less dramatic response to SAPCD2 depletion in terms of cell survival. While SAPCD2 depletion indeed resulted in a statistically significant reduction in cell viability in the KELLY cell line, the phenotypic consequence was less dramatic than what was observed in the BE(2)-C cell line. The most straightforward explanation for this difference is the likely possibility that SAPCD2 is naturally expressed at a lower level in the KELLY cell line compared to the BE(2)-C cell line. At lower basal expression levels, SAPCD2 depletion would reasonably result in a less dramatic cellular response compared to a cell line with higher basal expression levels. However, microarray expression data comparing multiple different neuroblastoma cell lines reveal that the difference in SAPCD2 expression levels between the two cell lines is not significant enough to account for the observed difference in phenotypic response (data not shown). The next likely explanation is the genetic heterogeneity of human cell lines. The BE(2)-C and KELLY cell lines have very unique genetic profiles with complex overlap between the expression levels of a magnitude of different genes. Higher expression levels of certain genes or activation of certain signaling pathways in the KELLY cell line, for example, might serve to attenuate or otherwise alter the phenotypic effect of SAPCD2 expression in a way that presents unique cellular responses to gene knockdown. This fact is also reflective of the clinical challenge

in developing anti-cancer therapies that are effective in all patients suffering from a specific cancer type. Although all neuroblastoma patients may share similar defining traits, each individual is genetically unique with expansive networks of signaling pathways that emphasize some phenotypes more than others. For this reason, it is important to investigate potential oncogenes across a panel of many unique human cell lines to account for these differences in cellular responses between individuals.

The effect of SAPCD2 knockdown on neuroblastoma cell proliferation was measured by colony formation assay in the BE(2)-C cell line. These proliferative assays serve as *in vitro* equivalents to *in vivo* tumor growth assays typically conducted in murine models. When cells are plated at very low densities, they form colonies in which size and number can be used as direct indicators of proliferation at the cellular level. In the BE(2)-C cell line, depletion of SAPCD2 led to a significant reduction in both colony size and number, suggesting that SAPCD2 functions in part to promote several different cellular events involved in sustaining proliferation. While these results were validated by two replicates in the BE(2)-C cell line, the KELLY cell line failed to produce any colonies within the expected time frame when plated at two separate cell densities. The inability of KELLY cells to produce colonies may also be reflective of unique genetic characteristics of this cell line, as colony formation relies upon the ability of the cells to maintain paracrine signaling in conditions of very low density. Colony formation is a direct measurement of tumorigenicity, which is sensitive to several characteristics inherent to the biochemistry of individual cell lines and may be

challenging or impossible to control in the laboratory setting. For this reason, the function of SAPCD2 as enhancing proliferative capacity in the BE(2)-C cell line should be explored in several others human neuroblastoma cell lines.

SAPCD2 is not directly involved in neuronal differentiation

Qualitative assessment of cell morphology is a reliable way to track differentiation status in neuronal precursors due to the unique morphological characteristics of neuronal cells. When fully differentiated, neural cells adopt small, star-shaped cell bodies and profound neurite outgrowth which may be readily detected under the microscope. However, poorly differentiated cells display large cell bodies with extensive clustering, irregular cell borders, and little to no neurite outgrowth. The obvious morphological differences between well-differentiated and poorly differentiated cells provides a simple, straightforward approach in detecting relative changes to differentiation status in response to gene knockdown. In the BE(2)-C cell line, SACPD2 depletion did not lead to a significant advancement in differentiation status compared to the differentiation-inducing agent miR-506-3p. These results were replicated in multiple different transfection experiments in the BE(2)-C cell line and later in the KELLY cell line. While SAPCD2 does not appear to play a direct role in modulating neuronal differentiation, there exists a possibility that it functions as one small effector within a complex web of genes involved in the differentiation pathway which could be modified and regulated through expression changes in several different genes at once. While this possibility may be worth future exploration, it is beyond

the scope of this thesis work.

V. CONCLUSION

Altogether, the results of this thesis work conclude that SAPCD2 likely functions as an oncogene in pediatric neuroblastoma. Retrospective clinical investigation of over 1,000 neuroblastoma patients revealed that children with higher expression levels of SAPCD2 have lower overall and event-free survival probabilities compared to children with lower expression levels of SAPCD2. Chromosomal amplification of the transcription factor and proto-oncogene MYCN similarly worsens prognosis in neuroblastoma and is a defining characteristic of high-risk cases. The regulatory relationship between MYCN and SAPCD2, if established, may present an important advancement in the identification of oncogenic pathways contributing to neuroblastoma.

In vitro biological experiments involved the use of two human neuroblastoma cell lines with distinct genetic and biochemical profiles. Both cell lines responded to SAPCD2 depletion with significant reductions in cell viability and one cell line with significant reductions in cell proliferation, further supporting the oncogenic role of SAPCD2 in neuroblastoma. While SAPCD2 may be involved in the regulation of apoptotic pathways, it does not appear to modulate neuronal differentiation. The results of this thesis work should be expanded upon in the future by the investigation of multiple new neuroblastoma cell lines to account for the vast genetic diversity of each individual case.

REFERENCES

1. Scalettar, B.A., et al., *Hindered submicron mobility and long-term storage of presynaptic dense-core granules revealed by single-particle tracking.* Dev Neurobiol, 2012. **72**(9): p. 1181-95.

2. Oronsky, B., et al., *Nothing But NET: A Review of Neuroendocrine Tumors and Carcinomas.* Neoplasia, 2017. **19**(12): p. 991-1002.

3. Barakat, M.T., K. Meeran, and S.R. Bloom, *Neuroendocrine tumours.* Endocr Relat Cancer, 2004. **11**(1): p. 1-18.

4. Patel, P. and K. Galoian, *Molecular challenges of neuroendocrine tumors.* Oncol Lett, 2018. **15**(3): p. 2715-2725.

5. Zarebczan, B. and H. Chen, *Signaling mechanisms in neuroendocrine tumors as targets for therapy.* Endocrinol Metab Clin North Am, 2010. **39**(4): p. 801-10.

6. Taal, B.G. and O. Visser, *Epidemiology of neuroendocrine tumours.* Neuroendocrinology, 2004. **80 Suppl 1**: p. 3-7.

7. Mitry, E., et al., *Treatment of poorly differentiated neuroendocrine tumours with etoposide and cisplatin.* Br J Cancer, 1999. **81**(8): p. 1351-5.

8. Marshall, G.M., et al., *The prenatal origins of cancer.* Nat Rev Cancer, 2014. **14**(4): p. 277-89.

9. Tomolonis, J.A., S. Agarwal, and J.M. Shohet, *Neuroblastoma pathogenesis: deregulation of embryonic neural crest development.* Cell Tissue Res, 2018. **372**(2): p. 245-262.

10. Simoes-Costa, M. and M.E. Bronner, *Establishing neural crest identity: a gene regulatory recipe.* Development, 2015. **142**(2): p. 242-57.

11. De Silva, D.C. and B. Wijesiriwardene, *The adrenal glands and their functions.* Ceylon Med J, 2007. **52**(3): p. 95-100.

12. Lotfi, C.F.P., et al., *The human adrenal cortex: growth control and disorders.* Clinics (Sao Paulo), 2018. **73**(suppl 1): p. e473s.

13. Sasano, H., et al., *Cell proliferation and apoptosis in normal and pathologic human adrenal.* Mod Pathol, 1995. **8**(1): p. 11-7.

14. Chang, S.P., et al., *Cell proliferation, movement and differentiation during maintenance of the adult mouse adrenal cortex.* PLoS One, 2013. **8**(12): p. e81865.

15. Mitani, F., *Functional zonation of the rat adrenal cortex: the development and maintenance.* Proc Jpn Acad Ser B Phys Biol Sci, 2014. **90**(5): p. 163-83.

16. Green, S.A., M. Simoes-Costa, and M.E. Bronner, *Evolution of vertebrates as viewed from the crest.* Nature, 2015. **520**(7548): p. 474-482.

17. Bronner, M.E. and N.M. LeDouarin, *Development and evolution of the neural crest: an overview.* Dev Biol, 2012. **366**(1): p. 2-9.

18. Betters, E., et al., *Analysis of early human neural crest development.* Dev Biol, 2010. **344**(2): p. 578-92.

19. Sauka-Spengler, T. and M. Bronner-Fraser, *A gene regulatory network orchestrates neural crest formation.* Nat Rev Mol Cell Biol, 2008. **9**(7): p. 557-68.

20. Louis, C.U. and J.M. Shohet, *Neuroblastoma: molecular pathogenesis and therapy.* Annu Rev Med, 2015. **66**: p. 49-63.

21. Brodeur, G.M., *Spontaneous regression of neuroblastoma.* Cell and tissue research, 2018. **372**(2): p. 277-286.

22. Fredlund, E., et al., *High Myc pathway activity and low stage of neuronal differentiation associate with poor outcome in neuroblastoma.* Proc Natl Acad Sci U S A, 2008. **105**(37): p. 14094-9.

23. Ruiz-Pérez, M.V., A.B. Henley, and M. Arsenian-Henriksson, *The MYCN Protein in Health and Disease.* Genes (Basel), 2017. **8**(4).

24. Trigg, R.M. and S.D. Turner, *ALK in Neuroblastoma: Biological and Therapeutic Implications.* Cancers (Basel), 2018. **10**(4).

25. Lee, C.C., et al., *Crystal structure of the ALK (anaplastic lymphoma kinase) catalytic domain.* Biochem J, 2010. **430**(3): p. 425-37.

26. Verma, P., S. Jain, and G. Kapoor, *Complete response with crizotinib in two children with chemotherapy resistant neuroblastoma.* South Asian J Cancer, 2017. **6**(2): p. 89-90.

27. Morales La Madrid, A., et al., *Targeting ALK: a promising strategy for the treatment of non-small cell lung cancer, non-Hodgkin's lymphoma, and neuroblastoma.* Target Oncol, 2012. **7**(3): p. 199-210.

28. Chen, Y., et al., *Oncogenic mutations of ALK kinase in neuroblastoma.* Nature, 2008. **455**(7215): p. 971-974.

29. Reynolds, C.P., et al., *Retinoid therapy of high-risk neuroblastoma.* Cancer Lett, 2003. **197**(1-2): p. 185-92.

30. Li, C., P.A. Einhorn, and C.P. Reynolds, *Expression of retinoic acid receptors alpha, beta, and gamma in human neuroblastoma cell lines.* Prog Clin Biol Res, 1994. **385**: p. 221-7.

31. Cheung, B.B., *Combination therapies improve the anticancer activities of retinoids in neuroblastoma.* World J Clin Oncol, 2015. **6**(6): p. 212-5.

32. Matthay, K.K., et al., *Treatment of high-risk neuroblastoma with intensive chemotherapy, radiotherapy, autologous bone marrow transplantation, and 13-cis-retinoic acid. Children's Cancer Group.* N Engl J Med, 1999. **341**(16): p. 1165-73.

33. Hämmerle, B., et al., *Targeting neuroblastoma stem cells with retinoic acid and proteasome inhibitor.* PLoS One, 2013. **8**(10): p. e76761.

34. Williams, G.H. and K. Stoeber, *The cell cycle and cancer.* J Pathol, 2012. **226**(2): p. 352-64.

35. Lischetti, T. and J. Nilsson, *Regulation of mitotic progression by the spindle assembly checkpoint.* Mol Cell Oncol, 2015. **2**(1): p. e970484.

36. Marston, A.L. and K. Wassmann, *Multiple Duties for Spindle Assembly Checkpoint Kinases in Meiosis.* Front Cell Dev Biol, 2017. **5**: p. 109.

37. Lawrence, K.S. and J. Engebrecht, *The spindle assembly checkpoint: More than just keeping track of the spindle.* Trends Cell Mol Biol, 2015. **10**: p. 141-150.

38. Marangos, P. and J. Carroll, *Securin regulates entry into M-phase by modulating the stability of cyclin B.* Nat Cell Biol, 2008. **10**(4): p. 445-51.

39. Maxwell, J.E., et al., *Somatic alterations of CDKN1B are associated with small bowel neuroendocrine tumors.* Cancer Genet, 2015.

40. Karpathakis, A., et al., *Prognostic Impact of Novel Molecular Subtypes of Small Intestinal Neuroendocrine Tumor.* Clin Cancer Res, 2016. **22**(1): p. 250-8.

41. Kim, H.S., et al., *p27 Loss Is Associated with Poor Prognosis in Gastroenteropancreatic Neuroendocrine Tumors.* Cancer Res Treat, 2014. **46**(4): p. 383-92.

42. Grabowski, P., et al., *Loss of nuclear p27 expression and its prognostic role in relation to cyclin E and p53 mutation in gastroenteropancreatic neuroendocrine tumors.* Clin Cancer Res, 2008. **14**(22): p. 7378-84.

43. Francis, J.M., et al., *Somatic mutation of CDKN1B in small intestine neuroendocrine tumors.* Nat Genet, 2013. **45**(12): p. 1483-6.

44. Shi, Y., et al., *Cell Cycle Protein Expression in Neuroendocrine Tumors: Association of CDK4/CDK6, CCND1, and Phosphorylated Retinoblastoma Protein With Proliferative Index.* Pancreas, 2017. **46**(10): p. 1347-1353.

45. Nie, J., et al., *Nusap1 is essential for neural crest cell migration in zebrafish.* Protein Cell, 2010. **1**(3): p. 259-66.

46. Verissimo, C.S., et al., *Neuroblastoma therapy: what is in the pipeline?* Endocr Relat Cancer, 2011. **18**(6): p. R213-31.

47. Shu, T., et al., *Doublecortin-like kinase controls neurogenesis by regulating mitotic spindles and M phase progression.* Neuron, 2006. **49**: p. 25-39.

48. Vreugdenhil, E., et al., *Doublecortin-like, a microtubule-associated protein expressed in radial glia, is crucial for neuronal precursor division and radial process stability.* European Journal of Neuroscience, 2007. **25**: p. 635-648.

49. Koizumi, H., T. Tanaka, and J. Gleeson, *Doublecortin-like kinase functions with doublecortin to mediate fiber tract decussation and neuronal migration.* Neuron, 2006. **49**: p. 55-66.

50. Fitzsimons, C., et al., *The microtubule-associated protein doublecortin-like regulates the transport of the glucocorticoid receptor in neuronal progenitor cells.* Molecular Endocrinology, 2008. **22**: p. 248-262.

51. Oltra, S., et al., *The doublecortin gene, a new molecular marker to detect minimal residual disease in neuroblastoma.* Diagnostic Molecular Pathology, 2005. **14**: p. 53-57.

52. Santra, M., et al., *Doublecortin induces mitotic microtubule catastrophe and inhibits glioma cell invasion.* Journal of Neurochemistry, 2009. **108**: p. 231-245.

53. Santra, M., et al., *Ectopic doublecortin gene expression suppresses the malignant phenotype in glioblastoma cells.* Cancer Research, 2006. **66**: p. 11726-11735.

54. Rihani, A., et al., *Inhibition of CDK4/6 as a novel therapeutic option for neuroblastoma.* Cancer Cell International, 2015. **15**(1): p. 76.

55. Partridge, V., et al., *Current Understanding on the Role of Cell Cycle Regulators in Neuroblastoma Cell Differentiation.* Med One, 2017. **2**(3): p. e170010.

56. Weng, Y.R., et al., *Role of C9orf140 in the promotion of colorectal cancer progression and mechanisms of its upregulation via activation of STAT5, beta-catenin and EZH2.* Carcinogenesis, 2014. **35**(6): p. 1389-98.

57. Xu, X., et al., *Identification and characterization of a novel p42.3 gene as tumor-specific and mitosis phase-dependent expression in gastric cancer.* Oncogene, 2007. **26**(52): p. 7371-7379.

58. Gifford, J.L., M.P. Walsh, and H.J. Vogel, *Structures and metal-ion-binding properties of the Ca2+-binding helix-loop-helix EF-hand motifs.* Biochem J, 2007. **405**(2): p. 199-221.

59. Liu, X., et al., *Application of intelligent algorithm in the optimization of novel protein regulatory pathway: Mechanism of action of gastric carcinoma protein p42.3.* J Cancer Res Ther, 2016. **12**(2): p. 650-6.

60. Donato, R., *Functional roles of S100 proteins, calcium-binding proteins of the EF-hand type.* Biochim Biophys Acta, 1999. **1450**(3): p. 191-231.

61. Newton, A.C., *Protein kinase C: poised to signal.* Am J Physiol Endocrinol Metab, 2010. **298**(3): p. E395-402.

62. Garg, R., et al., *Protein kinase C and cancer: what we know and what we do not.* Oncogene, 2014. **33**(45): p. 5225-37.

63. Tam, W.L., et al., *Protein kinase C α is a central signaling node and therapeutic target for breast cancer stem cells.* Cancer Cell, 2013. **24**(3): p. 347-64.

64. Zhang, J., et al., *p42.3 gene expression in gastric cancer cell and its protein regulatory network analysis.* Theoretical biology & medical modelling, 2012. **9**(1): p. 53-53.

65. Chen, P., et al., *Positive relationship between p42.3 gene and inflammation in chronic non-atrophic gastritis.* J Dig Dis, 2015. **16**(10): p. 568-74.

66. Cao, W.J., et al., *Overexpression of p42.3 promotes cell proliferation, migration, and invasion in human gastric cancer cells.* Tumour Biol, 2016. **37**(9): p. 12805-12812.

67. Luo, Y., et al., *Overexpression of SAPCD2 correlates with proliferation and invasion of colorectal carcinoma cells.* Cancer Cell Int, 2020. **20**: p. 43.

68. Hao, Y., et al., *Establishment of optimal regulatory network of colorectal cancer based on p42.3 protein.* Saudi J Biol Sci, 2017. **24**(8): p. 1781-1786.

69. Jia, X., et al., *Long noncoding RNA PXN-AS1-L promotes the malignancy of nasopharyngeal carcinoma cells via upregulation of SAPCD2.* Cancer Med, 2019. **8**(9): p. 4278-4291.

70. Liu, H., et al., *Depletion of p42.3 gene inhibits proliferation and invasion in melanoma cells.* J Cancer Res Clin Oncol, 2017. **143**(4): p. 639-648.

71. Li, P.H., et al., *p42.3 promotes cell proliferation and invasion in human Renal-Cell Carcinoma.* Int J Clin Exp Med, 2014. **7**(12): p. 4959-66.

72. Sun, W., et al., *Overexpression of p42.3 promotes cell growth and tumorigenicity in hepatocellular carcinoma.* World J Gastroenterol, 2013. **19**(19): p. 2913-20.

73. Cui, Y., et al., *MiR-29a inhibits cell proliferation and induces cell cycle arrest through the downregulation of p42.3 in human gastric cancer.* PLoS One, 2011. **6**(10): p. e25872.

74. Hao, Y., T. Fan, and K. Nan, *Optimization and Corroboration of the Regulatory Pathway of p42.3 Protein in the Pathogenesis of Gastric Carcinoma.* Comput Math Methods Med, 2015. **2015**: p. 683679.

75. Jung, Y., et al., *Clinical validation of colorectal cancer biomarkers identified from bioinformatics analysis of public expression data.* Clin Cancer Res, 2011. **17**(4): p. 700-9.

76. Yuan, X.S., et al., *p42.3: a promising biomarker for the progression and prognosis of human colorectal cancer.* J Cancer Res Clin Oncol, 2013. **139**(7): p. 1211-20.

77. Yang, J.D. and L.R. Roberts, *Epidemiology and management of hepatocellular carcinoma.* Infect Dis Clin North Am, 2010. **24**(4): p. 899-919, viii.

78. Wan, W., et al., *Differential expression of p42.3 in low- and high-grade gliomas.* World J Surg Oncol, 2014. **12**: p. 185.

79. Mao, L., et al., *Cell cycle-dependent expression of p42.3 promotes mitotic progression in malignant transformed cells.* Mol Carcinog, 2014. **53**(5): p. 337-48.

80. Qian, C.N., Y. Mei, and J. Zhang, *Cancer metastasis: issues and challenges.* Chin J Cancer, 2017. **36**(1): p. 38.

81. Chiu, C.W.N., et al., *SAPCD2 Controls Spindle Orientation and Asymmetric Divisions by Negatively Regulating the Galphai-LGN-NuMA Ternary Complex.* Dev Cell, 2016. **36**(1): p. 50-62.

82. Blumer, J.B., L.J. Chandler, and S.M. Lanier, *Expression analysis and subcellular distribution of the two G-protein regulators AGS3 and LGN indicate distinct functionality. Localization of LGN to the midbody during cytokinesis.* J Biol Chem, 2002. **277**(18): p. 15897-903.

83. Morin, X., F. Jaouen, and P. Durbec, *Control of planar divisions by the G-protein regulator LGN maintains progenitors in the chick neuroepithelium.* Nat Neurosci, 2007. **10**(11): p. 1440-8.

84. Konno, D., et al., *Neuroepithelial progenitors undergo LGN-dependent planar divisions to maintain self-renewability during mammalian neurogenesis.* Nat Cell Biol, 2008. **10**(1): p. 93-101.

85. Jiang, J., et al., *C9orf140, a novel Axin1-interacting protein, mediates the negative feedback loop of Wnt/β-catenin signaling.* Oncogene, 2018. **37**(22): p. 2992-3005.

86. MacDonald, B.T., K. Tamai, and X. He, *Wnt/beta-catenin signaling: components, mechanisms, and diseases.* Dev Cell, 2009. **17**(1): p. 9-26.

87. Hutchins, J.R., et al., *Systematic analysis of human protein complexes identifies chromosome segregation proteins.* Science, 2010. **328**(5978): p. 593-9.

88. Muniyappa, M.K., et al., *MiRNA-29a regulates the expression of numerous proteins and reduces the invasiveness and proliferation of human carcinoma cell lines.* Eur J Cancer, 2009. **45**(17): p. 3104-18.

89. Xu, H., et al., *MicroRNA miR-29 modulates expression of immunoinhibitory molecule B7-H3: potential implications for immune based therapy of human solid tumors.* Cancer Res, 2009. **69**(15): p. 6275-81.

90. Aravidis, C., et al., *Detection of numerical abnormalities of chromosome 9 and p16/CDKN2A gene alterations in ovarian cancer with fish analysis.* Anticancer Res, 2012. **32**(12): p. 5309-13.

91. Dagher, J., et al., *Histologic prognostic factors associated with chromosomal imbalances in a contemporary series of 89 clear cell renal cell carcinomas.* Hum Pathol, 2013. **44**(10): p. 2106-15.

92. Narayanan, V., et al., *Ponatinib for the treatment of chronic myeloid leukemia and Philadelphia chromosome-positive acute lymphoblastic leukemia.* Drugs Today (Barc), 2013. **49**(4): p. 261-9.

93. Kim, Y.I., et al., *Proteogenomic Study beyond Chromosome 9: New Insight into Expressed Variant Proteome and Transcriptome in Human Lung Adenocarcinoma Tissues.* J Proteome Res, 2015. **14**(12): p. 5007-16.

94. Liu, X., et al., *Maternal preconception body mass index and offspring cord blood DNA methylation: exploration of early life origins of disease.* Environ Mol Mutagen, 2014. **55**(3): p. 223-30.

95. Liu, H., et al., *A DNA vaccine targeting p42.3 induces protective antitumor immunity via eliciting cytotoxic CD8+T lymphocytes in a murine melanoma model.* Human vaccines & immunotherapeutics, 2013. **9**(10): p. 2196-2202.

96. Fire, A., et al., *Potent and specific genetic interference by double-stranded RNA in Caenorhabditis elegans.* Nature, 1998. **391**(6669): p. 806-11.

97. Morlando, M., et al., *Primary microRNA transcripts are processed co-transcriptionally.* Nature Structural & Molecular Biology, 2008. **15**(9): p. 902-909.

98. Wilson, R.C. and J.A. Doudna, *Molecular mechanisms of RNA interference.* Annu Rev Biophys, 2013. **42**: p. 217-39.

99. Tatiparti, K., et al., *siRNA Delivery Strategies: A Comprehensive Review of Recent Developments.* Nanomaterials (Basel), 2017. **7**(4).

100. Xu, C.-f. and J. Wang, *Delivery systems for siRNA drug development in cancer therapy.* Asian Journal of Pharmaceutical Sciences, 2015. **10**(1): p. 1-12.

101. Desai, S., et al., *Biological cytotoxicity evaluation of spiro[azetidine-2, 3'-indole]-2', 4(1'H)- dione derivatives for anti-lung and anti-breast cancer activity.* SCHOLAR RESEARCH LIBRARY, 2011. **3**: p. 236-243.

102. Lee, S. and D.K. Lee, *What is the proper way to apply the multiple comparison test?* Korean journal of anesthesiology, 2018. **71**(5): p. 353-360.

103. Bagatell, R., et al., *Significance of MYCN amplification in international neuroblastoma staging system stage 1 and 2 neuroblastoma: a report from the International Neuroblastoma Risk Group database.* Journal of clinical oncology : official journal of the American Society of Clinical Oncology, 2009. **27**(3): p. 365-370.

104. Chan, H.S., et al., *MYCN protein expression as a predictor of neuroblastoma prognosis.* Clin Cancer Res, 1997. **3**(10): p. 1699-706.

105. Zhao, Z., et al., *The PLAGL2/MYCN/miR-506-3p interplay regulates neuroblastoma cell fate and associates with neuroblastoma progression.* J Exp Clin Cancer Res, 2020. **39**(1): p. 41.

106. Desjardins, P. and D. Conklin, *NanoDrop microvolume quantitation of nucleic acids.* J Vis Exp, 2010(45).

107. Aranda, P.S., D.M. LaJoie, and C.L. Jorcyk, *Bleach gel: a simple agarose gel for analyzing RNA quality.* Electrophoresis, 2012. **33**(2): p. 366-9.

108. Greaves, M. and C.C. Maley, *Clonal evolution in cancer.* Nature, 2012. **481**(7381): p. 306-13.

109. Ngan, E.S., *Heterogeneity of neuroblastoma.* Oncoscience, 2015. **2**(10): p. 837-8.

110. Le Dréau, G., et al., *E proteins sharpen neurogenesis by modulating proneural bHLH transcription factors' activity in an E-box-dependent manner.* Elife, 2018. **7**.

111. Huang, M. and W.A. Weiss, *Neuroblastoma and MYCN.* Cold Spring Harb Perspect Med, 2013. **3**(10): p. a014415.

112. Wagner, E.M., *Monitoring gene expression: quantitative real-time rt-PCR.* Methods Mol Biol, 2013. **1027**: p. 19-45.

113. Han, H., *RNA Interference to Knock Down Gene Expression.* Methods Mol Biol, 2018. **1706**: p. 293-302.